Nanozyme-Engineered Liners for Proactive ~~Immunomodulation Against~~Prevention of Wear Particle-induced Osteolysis

Shujie Liu,[1] Sheng Zhao,[1,6] Qi Sun,[1,7] Quanyi Liu,[4,5] Yihong Zhang,[1] Yixuan Li,[2] Lifeng Jiang,[3] Tong Li,[1] Jianan Cao,[1] Jiansen Wang,[1] Jingyuan Zhao,[1] Xiaomiao Cui,[1] Jingjing Zhang[7], Xinkun Ren,[1] Yan Du, [4,5] Liming Zheng,[2,3] Qing Jiang,[2]* Hui Wei[1,7,8]**

[1] Department of Biomedical Engineering, College of Engineering and Applied Sciences, Nanjing National Laboratory of Microstructures, Jiangsu Key Laboratory of Artificial Functional Materials, Nanjing University, Nanjing, Jiangsu 210023, China.

[2] State Key Laboratory of Pharmaceutical Biotechnology, Division of Sports Medicine and Adult Reconstructive Surgery, Department of Orthopedic Surgery, Nanjing Drum Tower Hospital, The Affiliated Hospital of Nanjing University Medical School, Nanjing, Jiangsu 210008, China.

[3] Department of Orthopedic Surgery, the Second Affiliated Hospital, Zhejiang University School of Medicine, Hangzhou, Zhejiang, 310000, China.

[4] State Key Laboratory of Electroanalytical Chemistry, Changchun Institute of Applied Chemistry, Chinese Academy of Sciences, Changchun, Jilin 130022, China.

[5] School of Applied Chemistry and Engineering, University of Science and Technology of China, Hefei, Anhui 230026, China.

[6] Key Laboratory of Advanced Drug Delivery Systems of Zhejiang Province, College of Pharmaceutical Sciences, Zhejiang University, Hangzhou, Zhejiang 310058, China.

[7] State Key Laboratory of Analytical Chemistry for Life Science, School of Chemistry and Chemical Engineering, Chemistry and Biomedicine Innovation Center (ChemBIC), ChemBioMed Interdisciplinary Research Centre at Nanjing University, Nanjing University, Nanjing, Jiangsu 210023, China.

[8] Nanozyme Laboratory in Zhongyuan, Henan Academy of Innovations in Medical Science, Zhengzhou, Henan 451163, China.

*Corresponding authors.

E-mails: Liming Zheng, limzheng@zju.edu.cn; Qing Jiang, qingj@nju.edu.cn; Hui Wei, weihui@nju.edu.cn.

This PDF file includes:

~~Supplementary Notes~~

Experimental Procedures

Synthesis of ceria nanozyme-engineered ultra-high molecular weight polyethylene (CZPE)

Typically, 8 g of ultra-high molecular weight polyethylene (UHMWPE, LL-5040, Shanghai Lianle Chemical Industry Science and Technology Co., Ltd.) were dissolved in 1280 mL of decahydronaphthalene (Macklin) by stirring at 140 °C for 1 h to achieve complete polymer dissolution. Cerium acetylacetonate ($Ce(acac)_3$, Sigma-Aldrich) was then prepared at concentrations of 40 mg/mL in ethanol, with amounts of 205.38, 1070.13, and 2259.16 mg to fabricate the weight percentage of 1%, 5%, and 10% of CeO_2 in the resultant CZPE product. 5.13, 26.75, and 56.48 mL of $Ce(acac)_3$ ethanol solution was gradually and evenly introduced into the dissolved polyethylene solution, and the mixture was stirred at 140 °C for 24 h to promote the reaction. The resulting CZPE was poured into methanol at 0 °C, allowed to stand, and the organic solvent was decanted. The product was washed with ethanol, filtered, and dried under vacuum. PE samples were processed using the same protocol, excluding the addition of $Ce(acac)_3$.

Characterization of CZPE

Transmission electron microscopy (TEM) imaging of CZPE was carried out using a Tecnai 12 TEM instrument (Philips) operating at 120 kV. X-ray diffraction (XRD) patterns were measured by using the diffractometers (Ultima III, Rigaku and D8 advance, Bruker), utilizing Cu Kα radiation. The elemental distribution was analysed using energy-dispersive X-ray spectroscopy (EDS, Aztec X-MaxN 80, Oxford). X-ray photoelectron spectroscopy (XPS) spectra were acquired using a Nexsa G2 system (Thermo Scientific) with a monochromatic Al source. The crystallization behavior of CZPE and PE was evaluated by differential scanning calorimetry (DSC) test by utilizing a STA449F3A-0061M (NETZSCH) instrument. Thermodynamic parameters were calculated from the DSC thermograms. The enthalpy of crystallization (ΔH_c) of CZPE was obtained from the second crystallization curve. The degree of crystallinity for the PE component was calculated based on the crystallization peak area by using the following equation (1)[1]:

$$X_c(\%) = \frac{\Delta H_c}{(1-\varphi)\Delta H_m} 100 \quad (1)$$

where, ΔH_c is enthalpy of crystallization of the sample, ΔH_m is enthalpy of crystallization for 100% crystalline UHMWPE (293 J/g), and φ is the weight fraction of the CeO_2 in CZPE.

Fabrication of bulk PE and CZPE materials

CZPE with varying CeO_2 concentrations and PE were uniformly spread into stainless steel molds. The samples were compacted at room temperature to fill the mold cavities completely. Subsequent consolidation occurred through compression molding at 210 °C under 10 MPa for 15 min through a hot-pressing machine (YLJ-HP300, Kejing). The constructs were then cooled to room temperature at a rate of 5 °C/min.

Fabrication of bulk vitamin E-doped UHMWPE (VEPE) material

Aligning with the concentrations used in commercially available vitamin E-doped prosthetic devices, the mixture of UHMWPE and vitamin E (Aladdin) was prepared, at a mass concentration of 0.8% for vitamin E[2]. The blending process was followed by thermal pressing, employing the same molding conditions and procedural methodologies for bulk CZPE materials (vide supra).

Tensile strength measurement

Type 1B samples (n = 5 for each group) were stamped out of 4-mm-thin sections of the materials mentioned above according to ISO-527[3]. These samples were tested at a crosshead speed of 10 mm/min at room temperature on a universal testing machine (Instron-1121). The stress and strain were recorded at 10 Hz and the engineering stress–strain curves were calculated using the crosshead displacement. The ultimate tensile strength, yield strength, elongation at break were calculated.

Fracture toughness measurement

The notched Izod impact test samples (63.5 mm × 12.7 mm × 6.35 mm; n = 5) were double notched in accordance with ASTM-D256 standards and were impact fractured with an Izod

impact test machine (XJU-2.75, Chengde Testing Machine Factory)[4]. The energy loss of the pendulum after impact was recorded as the impact strength of the samples.

Tribological property measurement

The tribological properties of PE and CZPE samples (40 mm × 20 mm × 4 mm; n = 6) were measured with a UMT TriboLab (Bruker) using a linear reciprocating ball-on-plate configuration. Commercial ZrO_2 balls (4.8 mm diameter, Jinxiang) were used as counter-surfaces. The tests were carried out at 25 ± 3 °C and < 20% of relative humidity with the following parameters: stroke length of 10 mm, average sliding speed of about 2.48 cm/min, sliding time of 5400 s, and a normal applied load of 9 N. A new ball was used for each friction testing. The coefficient of friction and sliding time were recorded using a computer during the test.

The wear volume of the samples (W_V) was calculated as follows[5]:

$$W_V = \Delta x \times \mathrm{A} + \pi \frac{d^2}{8} W_1 \quad (2)$$

considering the sum of two terms: the first term represents the main W_V according to the ASTM G133 standard[6], which recommends measuring six 2D profiles for each track to determine the cross-section area beneath the 2D curves (A), and then multiplying those values by the nominal stroke (Δx). The second term is a correction factor that takes into account the two edges of the wear tracks. This term is assessed considering the width (d) and depth (W_1) of each wear track. The 2D track profiles were recorded with a stylus profiler (Dektak XT, Bruker).

The wear rate of the plates (W_R) was calculated according to ASTM G133 standard with the following equation:

$$W_R = \frac{W_V}{s \times F} \quad (3)$$

where F is the normal force and s the sliding distance.

Accelerated aging of bulk PE, CZPE, and VEPE samples

Sections of the bulk PE, CZPE, and VEPE samples were immersed in squalene (Meryer) at 120 °C for 24 h in a convection oven to allow the squalene to infuse into the polymer matrix. After immersion, all specimens were taken out and cooled to room temperature. Sample surfaces were then gently wiped with absorbent gauze to remove excess squalene. Afterwards, all samples are placed in an 80 ℃ convection oven for aging treatment for 4 months, ensuring maximum exposure to air. The accelerated aging time can be determined with the following equation according to ASTM F1980-07[7]:

$$Accelerated\ aging\ time = \frac{Desired\ real\ time}{Q_{10}^{\left[\frac{T_{AA}-T_{AMB}}{10}\right]}} \quad (4)$$

where Q_{10} is the aging factor (~2), T_{AA} is the accelerated aging temperature (80 ℃), and T_{AMB} is the ambient temperature. For the *in vivo* implantation, T_{AMB} was assumed to be the temperature of a human body (37 °C), and therefore the 4 months accelerated aging time is equivalent to *in vivo* working 6.~~56~~48 years.

Determination of oxidation stability

The aged samples were boiled in hexane (Sinopharm Chemical Reagent Co., Ltd) at 80 ℃ for 24 h and then vacuum dried for 24 h to remove any species, which could interfere with subsequent Fourier transform-infrared spectra (FT-IR) measurements. Infrared spectra were collected using a NICOLET iS50 FT-IR (Thermo Scientific) spectrometer with each spectrum recorded as an average of 32 individual infrared scans. Oxidation levels were quantified by an oxidation index described by ASTM F2102 as the ratio of the areas under 1680–1800 cm^{-1} to the absorbance over 1335–1390 cm^{-1} [8].

Preparation and characterization of particles

CZPE, and PE were subjected to mechanical grinding using a ball mill grinder (MSK-SFM-LN-192, MTI KJ Co., Ltd.) at a frequency of 50 Hz for 15 h to produce preliminary particles. The resulting particles were thoroughly washed with ethanol, and then subjected to gradient filtration using reusable filter units (300-4000, Nalgene) and filter membranes (Millipore) with pore sizes of 41, 20, 10, 5, and 0.01 μm to obtain particles with dimensions under 10 μm. The

particles were then preserved in ethanol and used for cellular and animal models. VEPE particles were prepared using the same procedure. To further analyze the size and morphology of the obtained particles, we filtered the particles again using filter membranes with pore sizes of 1 μm and 0.01 μm. The size and morphology of the particles were examined using a scanning electron microscope (SEM, Ultra 55, Zeiss). Subsequently, particle parameters such as equivalent circle diameter (ECD), aspect ratio (AR), and roundness (R) were quantified using ImageJ software[9].

Endotoxin levels were evaluated using a chromogenic LAL endotoxin assay kit (Genscript). A sample comprising 2 g of particles was immersed in 5 mL of LPS-free water for 24 h. Sterile filtration was conducted using a 0.22 μm filter head (Millipore) to remove particles. The filtrate was subsequently diluted fivefold with lipopolysaccharide (LPS)-free water. Both the undiluted and diluted solutions were subjected to endotoxin testing.

Preparation and characterization of CeO_2 nanoparticles

The synthesis of CeO_2 nanoparticles (NPs) was conducted following a previously published procedure[10]. Briefly, 504 mg $Ce(NO_3)_3 \cdot 6H_2O$ (J & K Scientific) was dissolved in 20 mL of ethylene glycol aqueous solution (v/v = 1:1) under vigorous stirring. The mixture was then heated to 60 °C while maintaining vigorous stirring. After 5 minutes, 4 mL of aqueous ammonia (28–30%) was rapidly added to the mixture. The reaction was allowed to proceed with continuous stirring for 3 hours. Subsequently, the products were collected by centrifugation, washed with excess deionized water. The CeO_2 NPs were dispersed in deionized water for further use and dried for characterization. The XPS spectrum and TEM images of CeO_2 NPs were obtained using the instruments described in the CZPE characterization section.

Measurement of hydroxyl radical scavenging activity

The formation of hydroxyl radicals (•OH) was facilitated through the Fenton reaction between Fe^{2+} and H_2O_2. The scavenging activity of •OH was quantitatively assessed using electron paramagnetic resonance spectroscopy (EPR, EMX PLUS, Bruker), based on the capture of •OH by the trapping agent 5,5-Dimethyl-1-pyrroline N-oxide (DMPO, J&K Chemical). H_2O_2

(Sinopharm Chemical Reagent Co., Ltd) and DMPO were premixed in PBS buffer (10 mM, pH 7.4), supplemented with 0.05% (v/v) poloxamer 188 (Sigma-Aldrich). Following this, the reaction was initiated by adding $FeSO_4$ (Sinopharm Chemical Reagent Co., Ltd) and allowed to proceed for 2 min before the addition of CZPE or PE particles. This subsequent reaction lasted for 10 s, after which the signal intensity was monitored immediately. The final concentrations of H_2O_2, Fe^{2+}, and particles were 2.5 mM, 2.5 mM and 200 μg/mL.

Measurement of SOD-Like Activity

The evaluation of the SOD-like activity of particles was conducted by quantifying their ability to scavenge superoxide anions ($O_2^{\bullet-}$), which was generated via light-induced irradiation of riboflavin (Sigma-Aldrich)[11]. Typically, 20 μL of riboflavin (1.2 mM), 80 μL of EDTA-2Na (0.1 M), 30 μL of nitrotetrazolium blue chloride (NBT, Sigma-Aldrich) probe (0.1 mg/mL), and 20 μL of particles suspensions at concentrations of 1 mg/mL, 2 mg/mL, and 5 mg/mL were added into 850 μL of PBS buffer (10 mM, pH 7.4). This mixture was then incubated at 37 °C for 5 min. Subsequent to the incubation, the solution was exposed to irradiation using a 27 W LED lamp for another 2 min. Finally, the absorbance of the solution at 580 nm was quantified through a microplate reader (Molecular Device).

Following a duration of one year of immersion in PBS buffer, the particles were then tested using the identical SOD-like activity protocols.

~~The SOD-like activity of recycled CZPE particles was measured following standard SOD-like activity protocols. After each test, the particles were washed with ethanol to remove riboflavin and NBT, then dried and re-dispersed before re-assessing their activity.~~

The SOD-like activity of CeO_2 NPs was measured according to standard SOD-like activity protocols, with the final concentrations of CeO_2 NPs in the test system set at 20, 40, and 100 μg/mL.

Measurement of CAT-Like Activity

The evaluation of CAT-like activity of the particles was performed through the quantification

of their catalytic efficiency in facilitating the decomposition of H_2O_2 to generate O_2. Typically, 1 mg/mL of the particles were added to a reaction mixture comprising 10 mM H_2O_2 in a 10 mM PBS buffer (pH 7.4), containing 0.05% (v/v) poloxamer 188. This particular concentration of poloxamer 188 was selected to optimize the dispersibility of PE and CZPE particles in the PBS medium, thereby reducing potential experimental inaccuracies. The resultant oxygen generation was quantified at specific time intervals of 0, 1.5, and 3 h using an oxygen electrode (SevenExcellence, Mettler Toledo). The final data were obtained by subtracting the background measured in PBS containing 0.05% (v/v) poloxamer 188 and 10 mM H_2O_2.

Subsequent to a duration of one year of immersion in PBS buffer, the particles were then tested using the identical CAT-like activity protocols.

~~The CAT-like activity of recycled CZPE particles was measured according to standard CAT-like activity protocols. After each test, PBS was carefully aspirated using a syringe, and the CZPE particles were dried, then re-dispersed for subsequent activity testing.~~

The CAT-like activity of CeO_2 NPs was measured according to standard CAT-like activity protocols, with the final concentrations of CeO_2 NPs in the test system set at 50 μg/mL.

Stability assessment of CZPE~~-5 particles and bulk CZPE~~ particle

Typically, 2 g of CZPE-5 particles were immersed in 10 mL of PBS (10 mM, pH 7.4). The containers were sealed with parafilm and left at room temperature for one year. Subsequently, 1 mL of the supernatant was diluted with deionized water to a final volume of 10 mL and filtered through a 0.01 μm pore size membrane to remove residual particles. The filtrate was then concentrated to 2 mL and digested with 6 mL of aqua regia on a hot plate at 250 °C until dry. The residue was dissolved in 10 mL of deionized water with ultrasonication. PBS that had been left standing under identical conditions for 1 year served as blank sample. The cerium (Ce) content was quantified using inductively coupled plasma mass spectrometry (ICP-MS, Agilent 7800).

To evaluate the catalytic stability of CZPE-5 particles, 200 mg of CZPE-5 was dispersed in 20

mL of deionized water containing 0.05% (v/v) poloxamer 188. H_2O_2 was then added to achieve a final concentration of 100 mM. The reaction system was placed on a shaker to proceed under constant agitation. At 24-hour intervals, aliquots of the reaction solution were carefully withdrawn using a syringe to minimize particle loss during sampling. The collected solution was subsequently filtered through a 0.22 μm membrane to remove residual particles. The absorbance of the filtrate at 240 nm was measured using a UV-Vis spectrophotometer (UV-3600Plus, Shimadzu) to quantify the residual concentration of H_2O_2. Subsequently, the concentration of Ce ions in the supernatant was determined by ICP-MS to evaluate the extent of CeO_2 NPs degradation within CZPE. After each measurement, H_2O_2 was replenished to restore its concentration to 100 mM, while maintaining a constant total reaction volume of 20 mL.

Cytotoxicity test

RAW264.7 and MT3T3-E1 cells were obtained from the Cell Bank of the Chinese Academy of Sciences. RAW264.7 cells were dispersed at a density of 6×10^5 cells/mL in a sodium alginate (Sigma Aldrich) solution with a mass concentration of 1.5%, which also contained 0.8 mg/mL of particles. After achieving a uniform dispersion, the mixture was incrementally added, at a rate of 30 μL per addition, into a ~~2.5% (w/v)~~100 mM $CaCl_2$ (Sigma Aldrich) solution to facilitate the formation of gel microspheres. The microspheres devoid of particles were fabricated as Ctrl group. These microspheres were then seeded in a 12-well plate at a density of eight microspheres per well, using Dulbecco's Modified Eagle Medium (DMEM, Gibco) supplemented with 10% Fetal Bovine Serum (FBS, Gibco). The medium was changed every two days. ~~Cell viability was assessed at 24, 72, and 120 h using the CCK-8 assay kit (Dojindo, Japan). The absorbance values (OD) at 450 nm of particles treated and Ctrl groups were measured. Cell viability (%) was calculated as follows:~~To establish a 2D monolayer Ctrl group, an equivalent number of RAW264.7 cells corresponding to the total cell number in eight microspheres per well was seeded directly into 12-well plates under the same culture conditions.

~~$$\text{Cell viability (\%)} = \left(\frac{OD_{\text{particles treated}} - OD_{\text{blank}}}{OD_{\text{Ctrl}} - OD_{\text{blank}}}\right) \times 100 \quad (5)$$~~

Cell proliferation was assessed at 24, 72, and 120 h using the CCK-8 assay kit (Dojindo, Japan), the optical density (OD) values at 450 nm of different experimental groups were measured using the same procedure. Briefly, CCK-8 solution was diluted in fresh culture medium at a ratio of 1:10. Then, 1.5 mL of the diluted solution was added to each well of a 12-well plate and incubated at 37 °C in a 5% CO_2 atmosphere for 30 min. After incubation, the absorbance at 450 nm was measured using a microplate reader. The diluted CCK-8 solution incubated under identical conditions without cells was used as the blank group. The ΔOD values for all experimental groups were calculated as follows:

$$\Delta OD = OD_{tested\ group} - OD_{blank} \quad (5)$$

The cytotoxicity assay of the particles on MC3T3-E1 cells was conducted following standard protocols. MC3T3-E1 cells were dispersed in sodium alginate solution at a concentration of 1×10^6 cells/mL, and then cultured in α-Minimum essential medium (α-MEM) supplemented with 10% FBS.

For the cytotoxicity assay of particles on fibroblasts, primary synovial fibroblasts were isolated from mice as follows: 8-week-old male ICR mice were euthanized by cervical dislocation and disinfected in 75% ethanol for 5 ~~minutes~~min. Under sterile conditions, the skin over the hindlimb knee joint was incised, and the surrounding synovial tissue was carefully excised and transferred to a sterile petri dish. The synovial tissue was minced into small fragments, and 0.2 mg/mL of type I collagenase (Biosharp) in DMEM was added for digestion. The mixture was incubated at 37 °C in a 5% CO_2 incubator for 6 hours. After digestion, the solution was centrifuged at 1000 rpm for 5 minutes, and the supernatant was discarded. The cells were resuspended in DMEM containing 10% FBS and cultured in incubator at 37 °C with 5% CO_2. Fibroblasts at passage 1 were used for the cytotoxicity assays, following the previously described protocol as RAW264.7 cells.

In vitro ROS-scavenging effect of CZPE particles

The *in vitro* ROS-scavenging effect of CZPE particles on cells was assessed using the inverted cell model. First, RAW264.7 cells were seeded at a density of 2×10^5 cells per well in a 12-

well plate and incubated for 12 h. CZPE and PE particles with concentrations of 0.2, 0.4, and 0.8 mg/mL were then dispersed in DMEM containing 10% FBS. This suspension was added to the wells, ensuring complete filling of each well, and sealed with parafilm. The plate was then inverted to maximize contact between the particles and cells. After 24 h of incubation, the plates were repositioned upright, and the medium containing particles was removed. The wells were washed thrice with PBS to eliminate residual particles. Cells were then incubated with 10 μM dichlorofluorescein diacetate (DCFH-DA, Sigma Aldrich) probe in the dark for 30 min, followed by the detection of intracellular ROS levels using flow cytometry (CytoFLEX, Beckman Coulter) and fluorescence microscopy (DMi8, Leica).

THP-1 cell culture and differentiation induction

THP-1 cells were a gift from Nanjing Drum Tower Hospital. THP-1 cells were seeded at a density of 2×10^6 cells per well in a 6-well plate and incubated for 12 hours. Differentiation was induced using 100 ng/mL of Phorbol 12-myristate 13-acetate (PMA) for 2 days. After observing the transformation of suspended THP-1cells into adherent macrophage cells, the PMA-containing medium was removed. The macrophage cells were then incubated in RPMI-1640 medium supplemented with 10% FBS for subsequent cell experiments.

The ROS scavenging assay of CZPE particles on THP-1-derived macrophages was performed according to the standard procedure, and fluorescence microscopy was used for detection.

Supernatant collection sorting for *in vitro* analysis

The macrophage supernatant induced by particle stimulation was generated using an inverted cell model, as previously described. The concentration of PE and CZPE particles used in this model was 0.8 mg/mL. After 24 hours of incubation, the plates were returned to an upright position, and the medium containing the particles was carefully collected. Excess particles were removed by centrifugation, and the resulting supernatant was aliquoted and stored at -80 °C. Subsequently, the cells that had been stimulated by the particles were harvested, washed three times with PBS, and stored at -80 °C for future use.

Culture and Stimulation of U266B1 Cells

U266B1 myeloma cells, sourced from the China Center for Type Culture Collection, were cultured in Roswell Park Memorial Institute (RPMI) 1640 medium (with 15% FBS) at 37 °C in a 5% CO_2 incubator. U266B1 cells were plated in six-well plates with 3×10^6 per well with different culture medium, including RPMI 1640 medium and a mixture medium of the RPMI 1640 medium and the supernatant from macrophages stimulated with various particles (1:1 dilution). The cells were cultured for four days, with medium changes every two days. Afterward, the cells were collected, washed three times with PBS, and stored at -80 °C for later use.

Osteoclast differentiation

Total bone marrow cells from 8-week-old male ICR mice were isolated by flushing the femur and tibia. The cells were plated in a cell dish overnight at 37 °C and 5% CO_2 with α-MEM medium containing 30 ng/mL macrophage colony-stimulating factor (M-CSF) and 10% FBS. After 24 hours, non-adherent bone marrow derived monocytes (BMMs) were collected, washed, and further cultured with the following mediums: osteoclast medium (α-MEM medium containing 10% FBS, receptor activator of nuclear factor kappa-B ligand (RANKL) and M-CSF), a mixture medium of the osteoclast medium and the supernatant from macrophages stimulated with various particles (1:1 dilution). The concentrations of RANKL and M-CSF in all medium were 50 ng/mL and 30 ng/mL, respectively. The culture medium was replaced every 2 days, and the cells were cultured until osteoclasts were observed under a microscope. Tartrate-resistant acid phosphatase (TRAP) staining ~~and qRT-PCR were~~was performed to evaluate osteoclast differentiation. The osteoclast area was quantified using ImageJ software.

Animal studies

All animal experiments were approved by the Institutional animal care and use committee (IACUC) of Nanjing University (IACUC-2209007). Institute of Cancer Research (ICR) mice were purchased from Beijing Vital River Laboratory Animal Technology Co., Ltd. NOD-*Prkdc*^{em1}*Il2rg*^{em2} (NCG) mice were purchased from Hangzhou Ziyuan Laboratory Animal

Technology Co., Ltd. All experimental mice were maintained in specific pathogen-free (SPF) conditions, with an ambient temperature of 24 ± 2 °C, air humidity of 40–70% and a 12 h dark/12 h light cycle. Throughout the study, mice were provided with autoclaved pellet food and water ad libitum.

For wear particle-induced calvaria osteolysis model, ~~PE and CZPE~~ particles stored in ethanol were filtered through a 0.01 μm membrane and resuspended in sterile FBS to a final concentration of 50 mg/mL (based on the weight of polyethylene). Eight-week-old male ICR mice were randomly divided into Ctrl, PE and CZPE groups, five mice per group. These mice were anesthetized and subjected to depilation, followed by a surgical incision measuring 2 cm over the calvaria. A 50 μL of suspension containing the particles was injected into the subperiosteal space of the calvarial sutures, followed by suture closure. The Ctrl group received only 50 μL of FBS. Post 14-day period, the animals were euthanized for subsequent examinations.

For the distal femur implant model, ~~PE, CZPE~~particles were resuspended in FBS as previously described. Medical-grade titanium alloy bone nails (JIURI), measuring 5 mm in length and 1 mm in diameter, were prepared by immersion in the particle-FBS suspension. Male ICR mice, 8 weeks of age, were randomly divided into Sham, Ctrl, PE, CZPE, VEPE and PE+CeO_2 groups (CeO_2 NPs were dispersed in the PE particle suspension at a concentration of 2.63 mg/mL, which is equivalent to the ~~cerium oxide~~CeO_2 content in the CZPE suspension), with eighteen mice in each group. These mice were anesthetized and depilated at the unilateral knee joint. A medial parapatellar arthrotomy was performed to expose the knee joint surface. A hole was drilled in the intercondylar fossa, followed by the injection of 20 μL of FBS suspension containing PE particles, CZPE particles, and PE particles + CeO_2 NPs, respectively. The titanium alloy bone pins were then inserted into the intramedullary canal, oriented parallel to the femoral shaft. An additional 20 μL of the particle-FBS suspension was administered into the hole, which was subsequently sealed with bone wax. The incision was closed with sutures. After 1, 4, and 7 weeks, the animals were euthanized for subsequent analysis.

For femoral implant model with U266B1 cell injection, eight-week-old male NCG mice were

randomly divided into six groups: Ctrl + PBS, Ctrl + U266B1, PE + PBS, PE + U266B1, CZPE + PBS, and CZPE + U266B1 groups, with six mice in each group. As previously detailed, the femoral distal implant model was firstly established in these mice. Commencing 4 weeks following particle implantation, U266B1 cells were subcutaneously injected at the implant site in a weekly sequence over three weeks. The U266B1 cells were prepared by centrifugation, resuspended in PBS to achieve a final concentration of 5×10^7 cells/mL, and 20 μL of this suspension was injected percutaneously near the implant site in the Ctrl + U266B1, PE + U266B1, and CZPE + U266B1 groups. The U266B1 cells were prepared by centrifugation and resuspended in PBS to a final concentration of 5×10^7 cells/mL. Subsequently, under the guidance of a portable X-ray machine, 20 μL of the cell suspension was injected into the bone marrow cavity via intramedullary injection in the Ctrl + U266B1, PE + U266B1, and CZPE + U266B1 groups. In Ctrl + PBS, PE + PBS, and CZPE + PBS, 20 μL of PBS was injected at the same site. At 7 weeks after surgery, the animals were euthanized for subsequent analysis.

For femoral distal implant model with bortezomib administration, eight-week-old male ICR mice were randomly divided into six experimental groups: Ctrl + PBS, Ctrl + Bortezomib, PE + PBS, PE + Bortezomib, CZPE + PBS and CZPE + Bortezomib groups, with six mice in each group. Follow the procedure described previously, the femoral distal implant model was firstly established. Commencing at week four post-implantation, the mice in Ctrl + Bortezomib, PE + Bortezomib, and CZPE + Bortezomib groups received intraperitoneal injections of 200 μL of PBS containing bortezomib (1 mg/kg, Solarbio) every 4 days for a total of 6 injections. In Ctrl + PBS, PE + PBS, and CZPE + PBS, 200 μL of PBS without bortezomib was intraperitoneally injected. The animals were euthanized at 7 weeks after surgery for further analysis.

Micro-CT analysis

Micro-CT scanning was performed using a VivaCT 80 scanner (SCANCO Medical AG, Switzerland) on calvarial and femoral tissues, post-soft tissue removal and fixation in 4% paraformaldehyde. The scanner settings were 45 kVp for voltage, 177 μA for current, and a voxel size of 15.6 μm. For calvaria, the region of interest (ROI) spanned 400 consecutive images starting from the disappearance of the anterior epiphyseal line. In the case of femurs,

the ROI encompassed 300 consecutive images in the proximal section of the osteo-epiphysis of the distal femur. Quantitative parameters, including bone volume to total volume (BV/TV), bone mineral density (BMD) of bone volume (BV), and BMD of total volume (TV), were calculated.

Histomorphometry measurement

Calvarias and femurs were fixed in 4% paraformaldehyde (Biosharp) for 24 h, followed by decalcification in a 10% ethylenediaminetetraacetic acid (EDTA, Sinopharm Chemical Reagent Co., Ltd) solution. Subsequent dehydration and transparency, the tissues were embedded in paraffin for sectioning. Sections of 5 μm thickness were stained using TRAP, hematoxylin and eosin (H&E, Servicebio), and Masson's trichrome (Servicebio). All sections were imaged with a Pannoramic MIDI slide scanner (3DHISTECH).

For the histomorphometry analysis of bone tissue, pathological parameters including bone formation (percentage osteoid perimeter, % O. Pm), bone resorption (percentage eroded perimeter, % Er. Pm), and osteoclast density (Number of Osteoclasts/Total Area, N.Oc/T.A) were identified and quantified in Masson and TRAP-stained sections as per established protocols[12]. For calvarias, the ROI was defined as the midline suture area, with three high-magnification fields randomly selected per mouse for averaging. For femurs, the ROI was identified as the trabecular bone area around the metal nail, with three high-magnification fields per mouse for statistical analysis.

In the assessment of tissue response to foreign body implantation, the pathological parameter quantified was the fibrous capsule thickness. This quantification was conducted on femoral sections stained with Masson’s trichrome. The ROI was identified as the fibrous capsule area surrounding the metal bone nail. Five mice per group, with each mouse having 6 regions randomly selected around the titanium alloy bone nails for analysis. The fibrous capsule thickness at these sites was quantified using the CaseViewer software. Considering the variability in the regions selected among individual mice, data points from individual mice were not averaged. Instead, all data were collectively displayed to assess inter-group differences.

Quantitative real-time polymerase chain reaction (qRT-PCR)

For cell samples, cells were collected by centrifugation. For tissue samples, seven weeks after the implantation of metal nails and particles, femoral bone from mice with the distal femur model were harvested. The bone nails were carefully removed, and excess tissue was trimmed, leaving only the tissue at the distal femur where the bone nails were inserted. Total RNA was extracted using Trizol reagent (Servicebio #G3013). Complementary DNAs were synthesized using the SweScript All-in-One RT SuperMix Kit (Servicebio #G3337). QRT-PCR amplifications were performed on an Applied Biosystems StepOne™ real-time PCR (Thermo Scientific) machine using Universal Blue SYBR Green qPCR Master Mix (Servicebio # G3326), following the manufacturer's protocol. The expression levels of mouse mRNA were normalized to the *Gapdh* gene, while human mRNA expression was normalized to the *GAPDH* gene. The relative abundance of each gene was calculated by subtracting the CT value of each sample for an individual gene from the corresponding CT value of *Gapdh* or *GAPDH* (ΔCT). ΔΔCT values were calculated by subtracting the ΔCT of the reference group from the ΔCT of the experimental group. -ΔΔCT values were then raised to the power 2 ($2^{-\Delta\Delta CT}$) to determine the fold-change in gene expression relative to the reference group. Each experiment was repeated at least three times. The sequences of primer set for mRNA are shown in Supplementary Table 3.

Western blotting

The tissue collection procedure was performed as described in the qRT-PCR experiment section above. The tissue was placed in a 1.5 mL EP tube without enzyme, and 300 μL of RIPA lysis buffer (Servicebio #G2002) was added. The tissue was then homogenized using a SWE-FP high-speed tissue grinder (Servicebio). Afterward, the EP tube was incubated at 4 °C for 40 minutes, followed by centrifugation at 12,000 rpm at 4 °C for 5 minutes. The supernatant was then collected. The supernatant was diluted with 5× sodium dodecyl sulfate polyacrylamide (SDS-PAGE) protein loading buffer (Servicebio #G2075), and heated at 100 °C for 5 minutes to obtain the protein storage solution. Proteins were separated using 15% SDS-PAGE gels and transferred onto polyvinylidene fluoride (PVDF) membranes. The PVDF membranes were

blocked at room temperature for 1 hour using PBS containing 0.1% Tween 20 (PBST) with 5% non-fat dry milk. The membranes were then incubated overnight at 4 °C with specific primary antibodies. After washing, the membranes were incubated with HRP-conjugated goat anti-rabbit IgG antibody (Beyotime #A0208) in 1% non-fat dry milk-PBST for 2 h at room temperature for 2 hours. Following additional washing with PBST, the blots were visualized using an ECL kit (Servicebio #G2014) on a Tanon 5200 Multi Chemiluminescent Imaging System (Tanon). Western Blot signals were quantified using ImageJ software. Antibodies were as follows: primary antibody against CD138 (Rabbit, Abcam #ab128936), recombinant anti-beta actin (β-actin) antibody (HRP conjugated, Servicebio ZB15001-HRP).

Immunofluorescence staining and analysis

Embedded tissue samples were sectioned at 5 μm thickness, mounted onto glass microscope slides, and air-dried at 42 °C overnight. The slides were deparaffinized, rehydrated, and subjected to antigen retrieval using a 10 mM sodium citrate buffer (pH 6) with heat mediation. Following three washes in PBS, slides were blocked using a solution of 3% bovine serum albumin in PBS for 1 h. This was followed by incubation in the dark with primary antibodies (anti-interleukin-1 beta (IL-1β) antibody, Rabbit, Servicebio #GB11113, 1:800; anti-CD138 antibody, Rabbit, Abcam #ab128936, 1:3000; anti-B220 antibody, Rabbit, Servicebio #GB113886, 1:300; anti-interleukin-6 (IL-6) antibody, Rabbit, Servicebio #GB11117, 1:500; anti-tumor necrosis factor-α (TNF-α) antibody, Rabbit, Servicebio #GB11188 , 1:200; anti-alpha smooth muscle actin (α-SMA) antibody, Rabbit, Servicebio #GB111364, 1:300) at room temperature for 8 h, and subsequently with corresponding secondary antibodies and 4′,6-diamidino-2-phenylindole dihydrochloride (DAPI; Servicebio, #G1012) for 1 h. Post antibody incubation, each slide was washed 3 times in PBS. The slides were then cover slipped.

Immunofluorescence slides were scanned using a Pannoramic MIDI slide scanner. For the quantification of IL-1β, IL-6, and TNF-α intensity, ROIs in were defined as previously described. Three high-magnification fields per mouse were randomly selected for statistical analysis. Fluorescence intensity was quantified using ImageJ software. For the assessment of $CD138^{+}/B220^{-}$ cell density, the ROI was designated as the bone marrow cavity surrounding the

metal bone nail. For the assessment of α-SMA$^+$ cell density, the ROI was defined as the fibrous tissue surrounding the metal bone nail. The number of target cells and the area of the ROI were quantified using CaseViewer software.

Particle distribution analysis

The distribution of CZPE and PE particles in femoral H&E-stained sections was observed using a polarizing microscope (Eclipse LV100N POL, Nikon), as previously described. To differentiate CZPE and PE particles from artifacts, the following criteria were applied[~~13~~13]: (1) poor visualization or indistinct identity under plain light, (2) strong birefringence and silver-white appearance without dichroism under polarized light, (3) presence within or surrounding histiocytes, and (4) location within the focal plane of cell cytoplasm.

Key metabolic tissues (heart, liver, spleen, lung, and kidney) and femurs were harvested, air-dried, and weighed. The tissues were then homogenized in aqua regia, and the ~~cerium~~Ce content was quantified using Inductively Coupled Plasma Optical Emission Spectrometry (ICP-OES, iCAP 7200, Thermo /Avio 220 Max, PerkinElmer). The ~~cerium~~Ce content in visceral tissues was calculated per unit mass. The ~~cerium~~Ce content in the femurs was calculated based on the total mass of the femur.

Biocompatibility assessment

To assess the biocompatibility of CZPE, various organs, including the heart, liver, spleen, lung, and kidney, were harvested from mice post-exposure. The tissues were sectioned and stained with H&E. These sections were subsequently imaged using a Pannoramic MIDI slide scanner for analyzing inflammatory responses and structural alterations. The same methodology was applied to investigate the principal visceral changes induced by bortezomib and U266B1 cells.

Evaluation of bortezomib toxicity on peripheral blood cells

8-week-old male ICR mice were administered a 200 μL intraperitoneal injection of PBS containing bortezomib (1 mg/kg). Mice injected with pure PBS were used as the Sham group. Injections were performed every four days, for a total of six injections. On the day following

the final injection, peripheral blood was collected from the orbital sinus, using a capillary tube, and stored in anticoagulant tubes. Cell counting was subsequently performed using a BC-2800vet automatic cell analyzer (Mindray).

Transcriptome sequencing and data analysis

Femurs from the distal femoral implant model mice were harvested, with peripheral soft tissues carefully removed. The specific segment of the femur encompassing the bone nail insertion area was then prepared for transcriptome sequencing. Transcriptome sequencing was performed by Shanghai OE Biotech Co., Ltd (Shanghai, China). Total RNA was extracted using the RNeasy Lipid Tissue Mini Kit (QIAGEN, 74804) according to the manufacturer's protocol. RNA purity and concentration were assessed using a NanoDrop 2000 spectrophotometer (Thermo Scientific), while RNA integrity was evaluated using a 2100 Bioanalyzer (Agilent). Libraries were constructed utilizing the VAHTS Universal V6 RNA-seq Library Prep Kit for Illumina (NR604, Vazyme) as per the manufacturer's instructions. Sequencing was performed on an Illumina Novaseq 6000 system (Illumina), generating 150 bp paired-end reads.

Initial processing of raw fastq format reads was executed using Fastp, with low-quality reads removed to acquire clean reads. These clean reads were then aligned to the reference mouse genome using HISAT2. Gene expression levels were quantified as FPKM, and read counts for each gene were determined using HTSeq-count. Differential expression analysis was conducted using DESeq2, with a threshold for differentially expressed genes (DEGs) set at Q value < 0.05 and $|\log_2^{foldchange}\log_2^{fold\ change}| > 1$. Hierarchical cluster analysis of DEGs was carried out to illustrate gene expression patterns across different groups and samples. Gene Set Enrichment Analysis (GSEA) was performed using GSEA software, ranking genes based on differential expression and testing for enrichment of predefined gene sets at the top or bottom of this ranking.

Statistical analysis

For quantitative analysis, the replicates were indicated in the corresponding figure legends. Statistical analysis was performed with GraphPad Prism v.8.4.3. and Microsoft Excel 2021.

The version of ImageJ software used is Fiji 15.4d. The results are expressed as mean ± s.d. Data were analysed by unpaired t-test, one-way analysis of variance (ANOVA) with Tukey's multiple comparison test, two-way ANOVA with Tukey's multiple comparison test. A *P* value <0.05 was considered statistically significant.

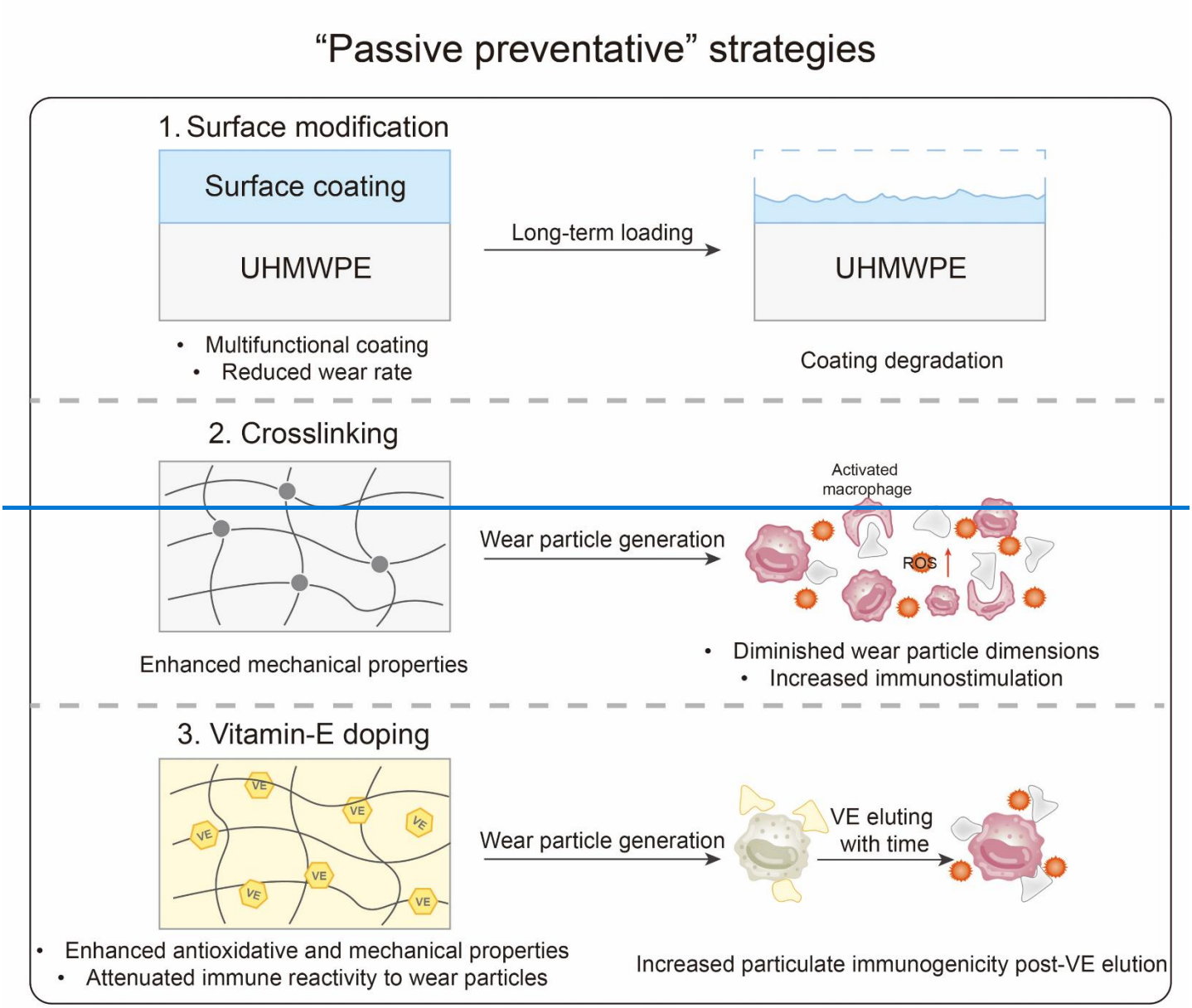

~~Supplementary Fig. 1 | Characteristics of "passive preventative" strategies.~~

Supplementary Note 1

The choice of cell culture model is critical for accurately evaluating the stimulatory effects of particles on cells. Due to the buoyancy of polymeric particles, conventional upright (2D/ monolayer) culture systems often fail to ensure sufficient contact between particles and adherent cells[14]. Furthermore, widely used inverted models present practical limitations, particularly in long-term culture, due to the difficulty of medium exchange[15]. To address the challenges of ensuring close contact between particles and cells while also supporting long-term culture, we employed a three-dimensional alginate microsphere model to investigate particle-induced cytotoxicity (Supplementary Fig. 14a).

We first compared cellular proliferation in alginate microspheres versus traditional 2D monolayers. As shown in Supplementary Fig. 14b-d, the 3D alginate bead Ctrl group consistently exhibited lower ΔOD (450 nm) values compared to the 2D monolayer Ctrl group across all time points, suggesting a slower proliferation rate in the 3D system. This effect is likely attributable to the restricted cell migration and spreading within microspheres, which reduces mitotic efficiency[16]. Nonetheless, ΔOD values in the 3D Ctrl group steadily increased over time for all tested cell types, indicating that the alginate microsphere system provides a sufficiently supportive environment for cell survival and proliferation during extended culture.

Furthermore, we observed that under 3D microsphere culture conditions, cell proliferation in the PE particle-treated group also increased over the course of cultivation, although to a lesser extent than in the Ctrl and CZPE groups. This trend may be attributed to a dynamic cellular response to particle exposure. During the initial 24 hours of co-culture, cells likely experienced the strongest stimulation, leading to reduced viability. However, due to the low initial seeding density, the cells retained sufficient space for proliferation. Cells that were not in direct contact with the particles were subjected to weaker stimulation and thus preserved their proliferative capacity. Nevertheless, the enhanced immunostimulatory effects of PE particles likely contributed to the lowest overall proliferation rate. In contrast, the CZPE group exhibited a partial recovery of proliferative capacity, suggesting that CZPE particles exerted less interference with normal cellular physiological functions. Moreover, the ΔOD values of all three cell types in the 2D monolayer Ctrl group initially increased and then declined, suggesting that cell proliferation was followed by a degree of cell death. This pattern is likely attributable to cellular crowding[17] and contact inhibition[18] under high-density conditions. Although cell proliferation in the 3D culture system may be slower than in conventional 2D models, the alginate microsphere model offers a more physiologically relevant platform for evaluating the long-term cytoprotective effects of different particles.

Supplementary Note 2

Currently, no commercially available product has been specifically developed to prevent aseptic loosening by regulating the local inflammatory microenvironment. The only clinically applied design that may provide some improvement in immunostimulatory properties is VEPE[2]. It is widely accepted that vitamin E exerts its antioxidant function during the processing of UHMWPE by scavenging free radicals, thereby delaying oxidative degradation of the material over time[19]. Accordingly, the original design intent of VEPE was primarily to enhance the mechanical stability of UHMWPE[19]. The observed reduction in immunostimulatory activity is mainly attributed to the passive release of the small-molecule antioxidant vitamin E, the effectiveness of which may gradually diminish due to elution and depletion over time[20]. Based on this background, we performed a comparative evaluation of the preventive efficacy of CZPE and VEPE particles against WPO[21]. The VEPE particles were fabricated using the same procedure as the CZPE particles. As shown in Supplementary Fig. 25, at the one-week time point, the VEPE group showed superior inhibition of bone resorption compared to the CZPE group, likely due to the antioxidant properties of vitamin E. This reduction in bone resorption was maintained until week 4. However, after week 4, the VEPE group exhibited a significant decrease in BV/TV, BMD of BV, and BMD of TV compared to the CZPE group, indicating an acceleration in bone resorption. These results suggest that although VEPE particles exhibit stronger early-stage suppression of osteoclast activation, their long-term preventive potential may be limited by the elution and loss of small molecules. In contrast, CZPE particles displayed a more sustained preventive effect.

Although some prosthetic design strategies have incorporated small molecules such as antibiotics into UHMWPE to achieve controlled release, these approaches are primarily intended for the rapid management of periprosthetic joint infection[22,23]. However, they are not well aligned with the therapeutic requirements for long-term inflammation control in the context of aseptic loosening[24]. Against this backdrop, the incorporation of long-acting antioxidants to attenuate the immunostimulatory effects of UHMWPE wear particles presents a novel design strategy for the development of next-generation prostheses aimed at preventing aseptic loosening.

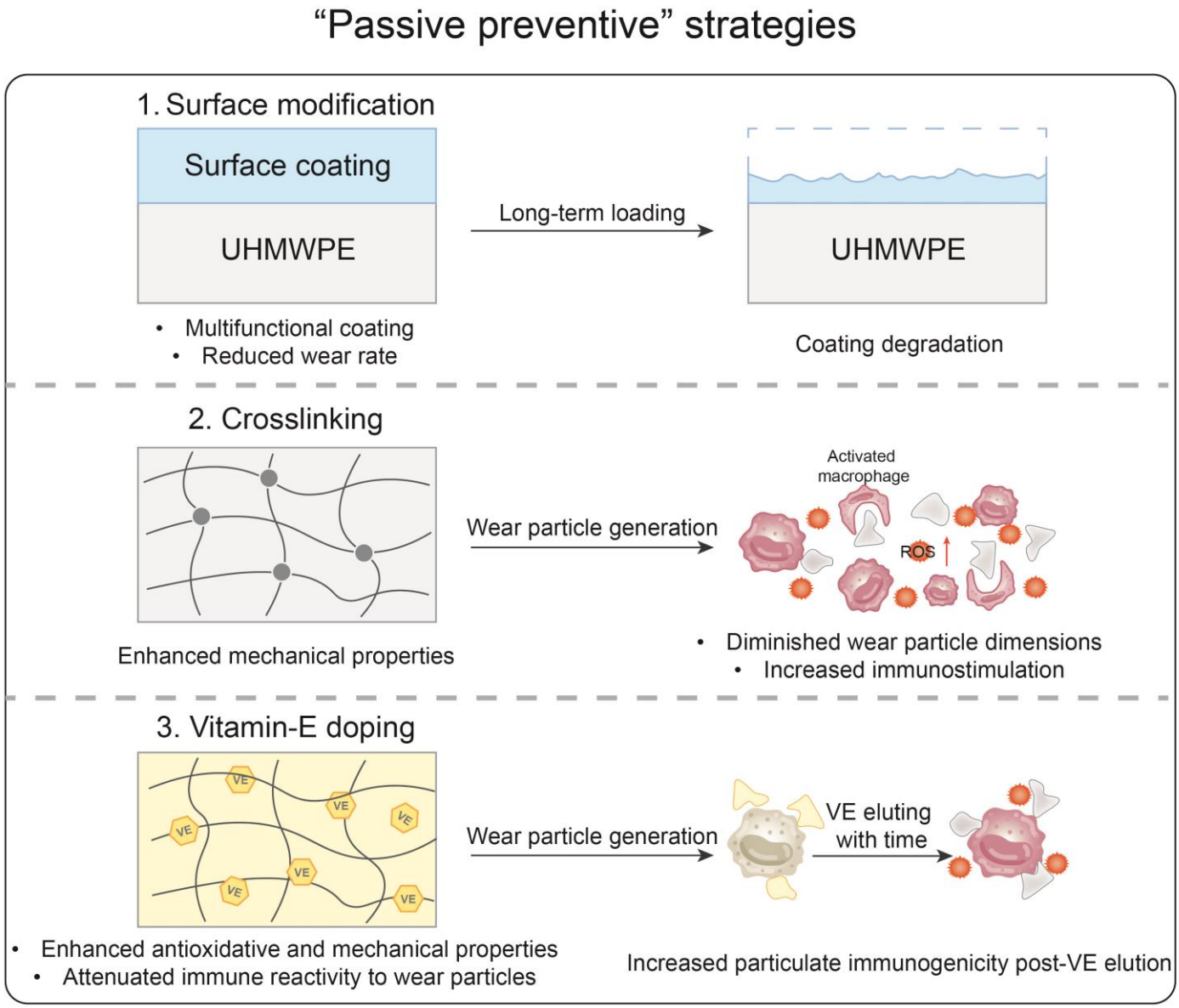

Supplementary Fig. 1 | Characteristics of "passive preventive" strategies.

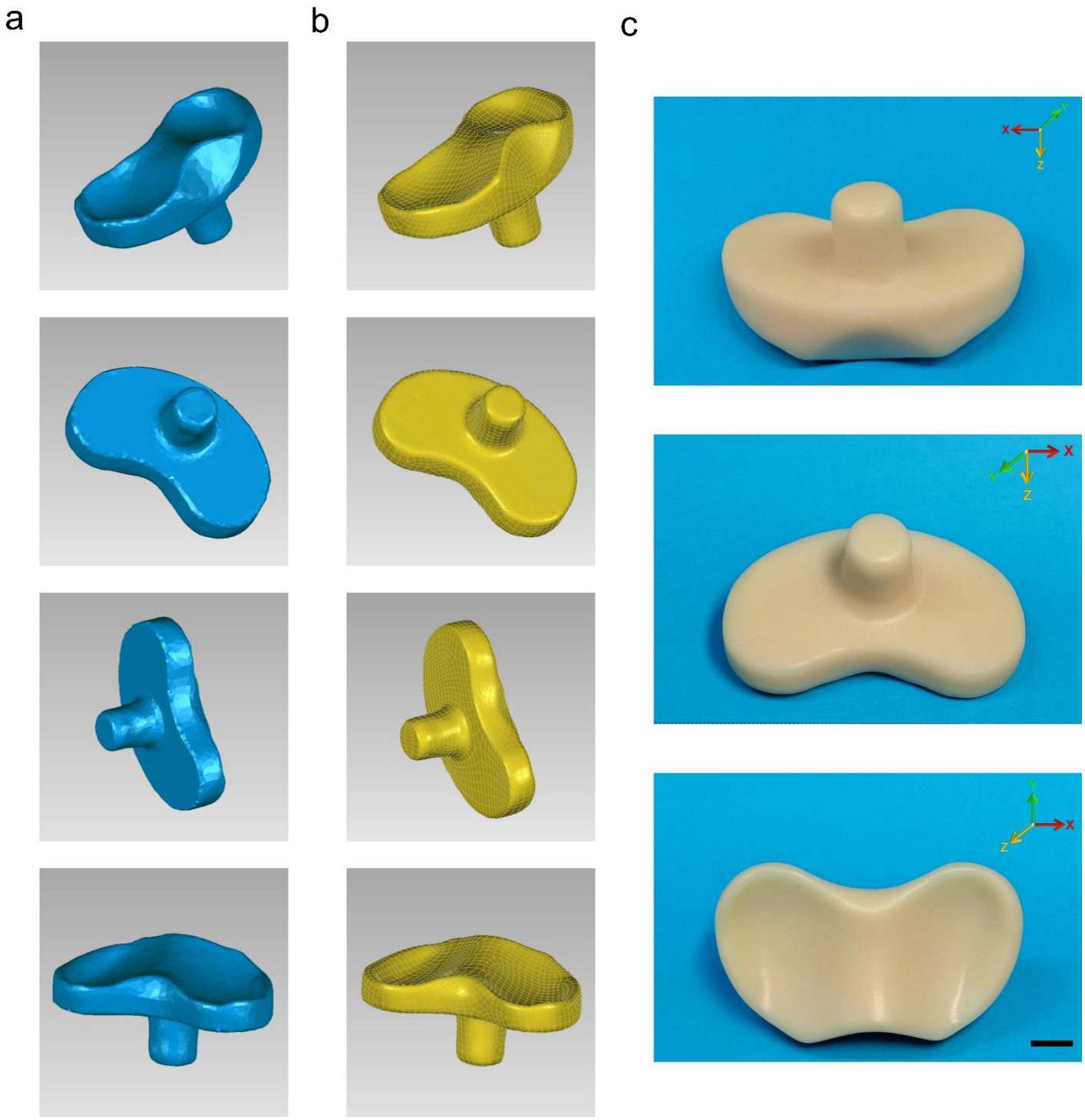

Supplementary Fig. 2 | Fabrication process of knee joint prosthesis. a, Preliminary encapsulation of 3D model after redundant data removal. **b**, 3D model after fitting surfaces and smoothing treatment. **c**, Photos of a knee joint liner fabricated using computer numerical control machining based on the model in **b**. Scale bar, 1 cm.

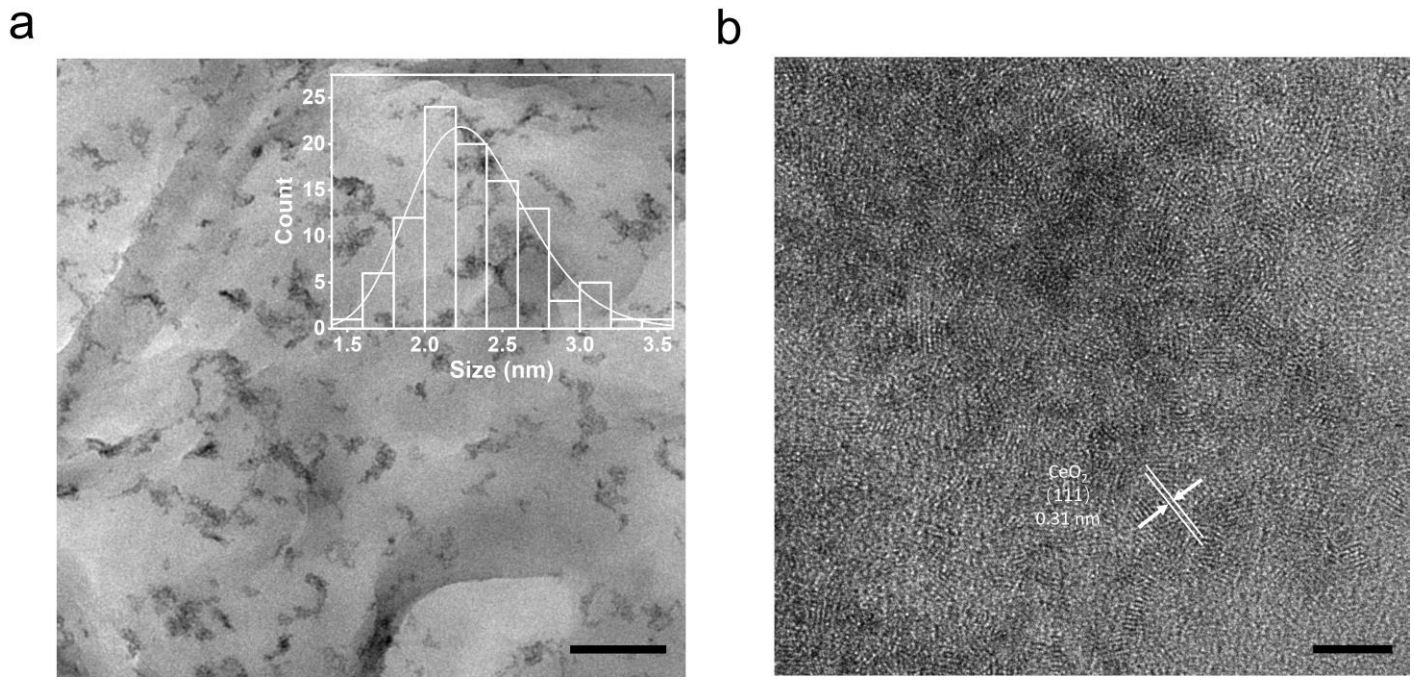

Supplementary Fig. 3 | TEM images of CeO_2 in PE matrix. a, TEM image of CeO_2 particles dispersed in PE. Scale bar, 50 nm. Inset: the corresponding size distribution measured by Image J. **b**, Magnified TEM image showing the (111) plane of CeO_2 with a 0.31 nm interplanar distance. Scale bar, 5 nm.

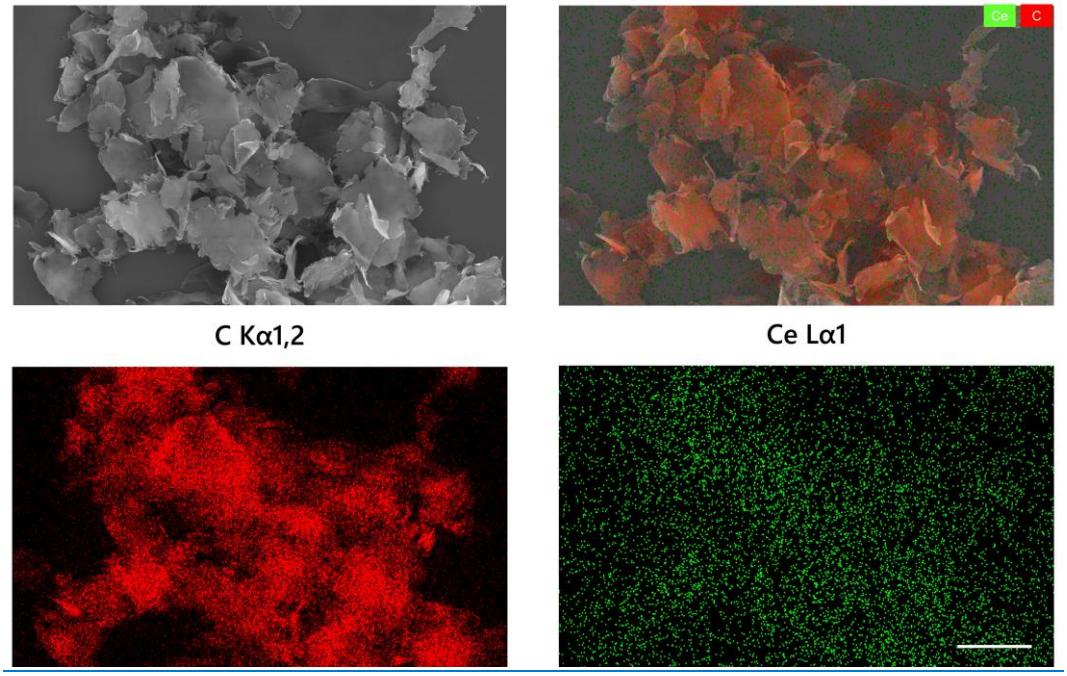

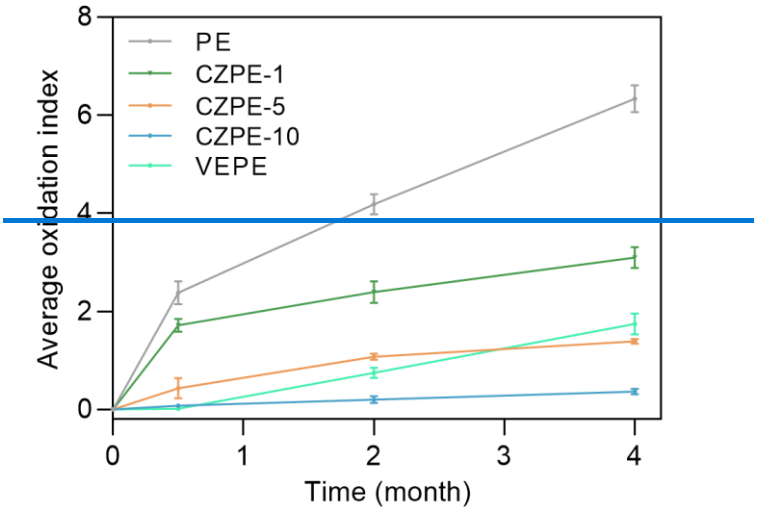

Supplementary Fig. 4 | Distribution of Ce element in CZPE particles. Green indicates Ce, and red indicates carbon. Scale bar, 25 μm.

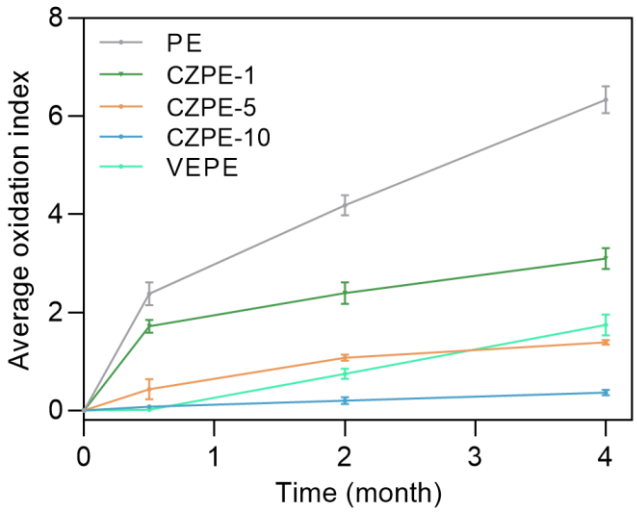

Supplementary Fig. 5 | Oxidation index variation over time. Temporal evolution of oxidation indices for bulk CZPE-1, CZPE-5, CZPE-10, PE, and VEPE samples at 0.5, 2, and 4 months (n = 6). Data are presented as mean ± s.d.

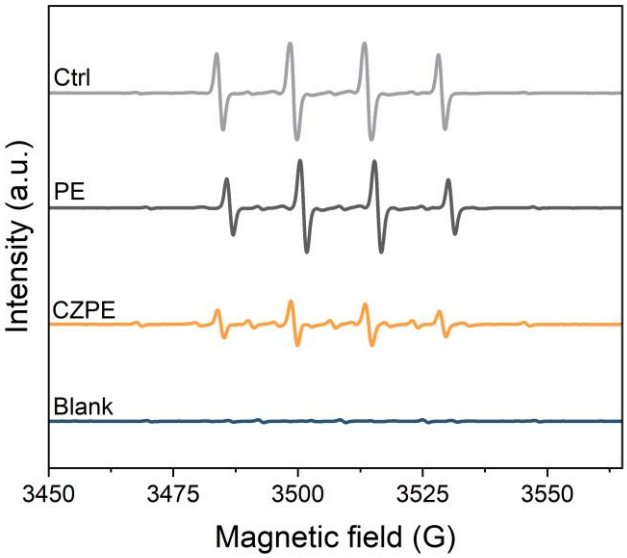

Supplementary Fig. ~~5~~6 | Scavenging capacity for ˙OH by CZPE and PE. Detection by electron paramagnetic resonance (EPR) analysis.

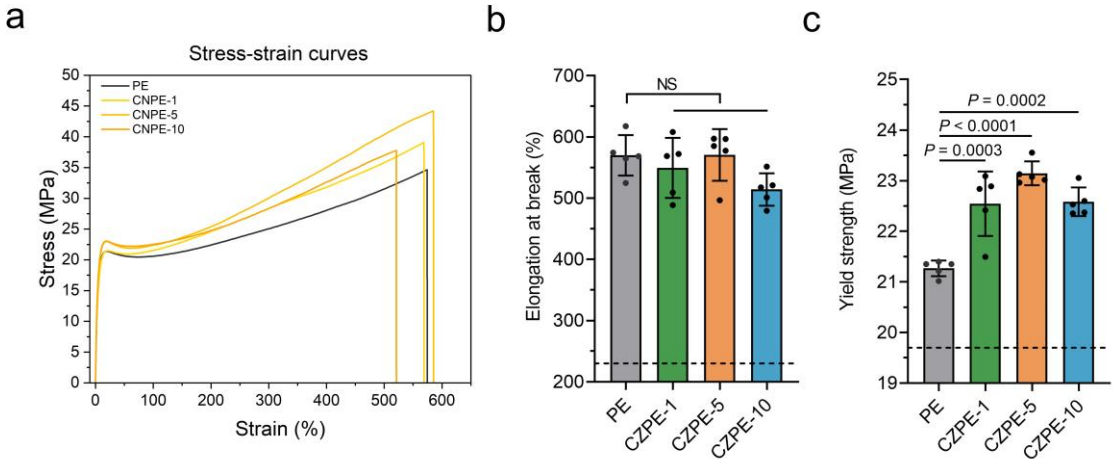

Supplementary Fig. 67 | Tensile properties of bulk CZPE-1, CZPE-5, CZPE-10, and PE. a, Representative stress-strain curves. **b**, Elongation at break (n = 5). **c**, Yield strength (n = 5). Dotted line indicates the minimum value of clinically used UHMWPE. Data in **b, c** are presented as mean ± s.d. P values were analysed by one-way ANOVA with Tukey's multiple comparisons test. NS, not significant, $P \geq 0.05$.

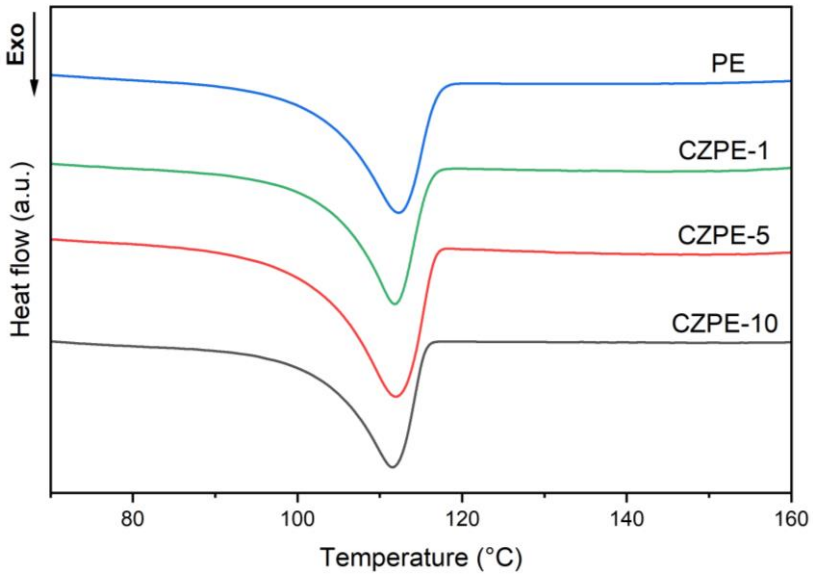

Supplementary Fig. ~~7~~8 | Differential scanning calorimetry (DSC) traces of CZPE-1, CZPE-5, CZPE-10, and PE materials.

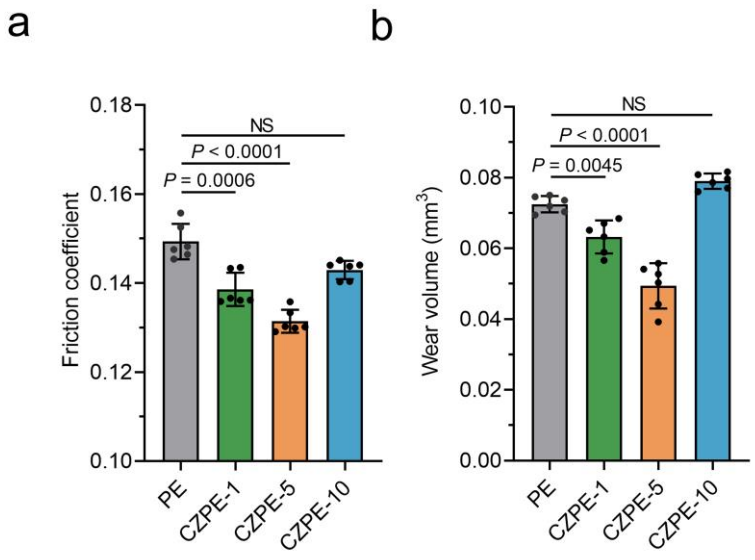

Supplementary Fig. 89 | Tribological testing for wear resistance of bulk CZPE-1, CZPE-5, CZPE-10, and PE. a, Friction coefficient in the steady-state region (n = 6). **b**, Wear volumes (n = 6). Data are presented as mean ± s.d. P values were analysed by one-way ANOVA with Tukey's multiple comparisons test. NS, not significant, $P \geq 0.05$.

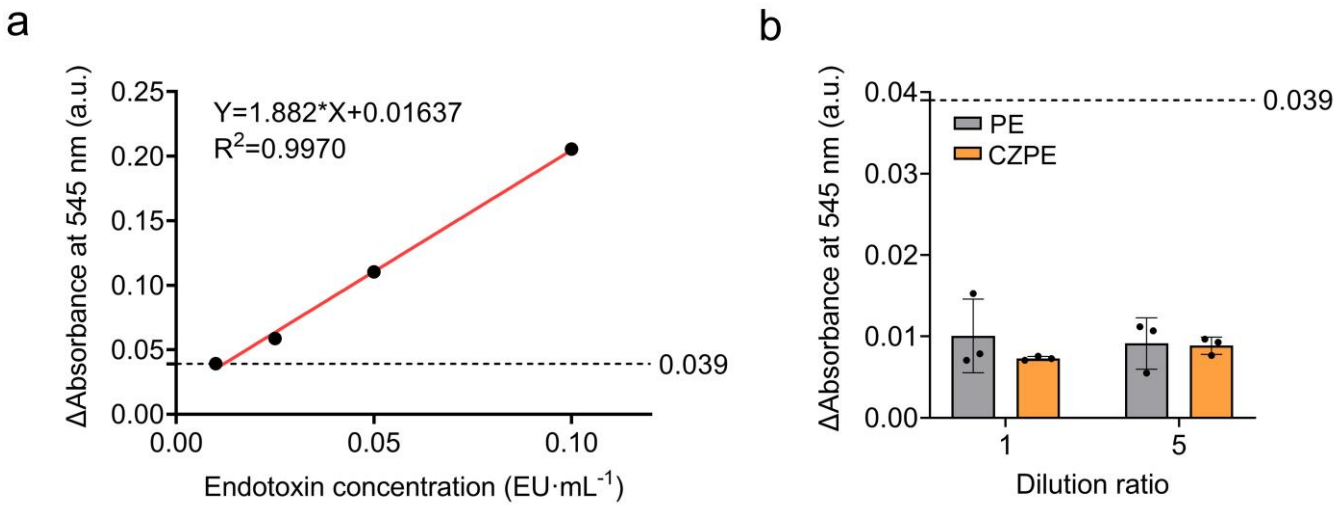

Supplementary Fig. ~~9~~10 | Evaluation of endotoxin content using a chromogenic limulus amebocyte lysate (LAL) endotoxin assay kit. a, Standard curve for endotoxin detection established by the chromogenic assay kit. **b**, Endotoxin levels in material extracts at various dilutions (n = 3). Measured endotoxin concentrations were below the minimum detectable limit of the standard assay kit. Data are presented as mean ± s.d.

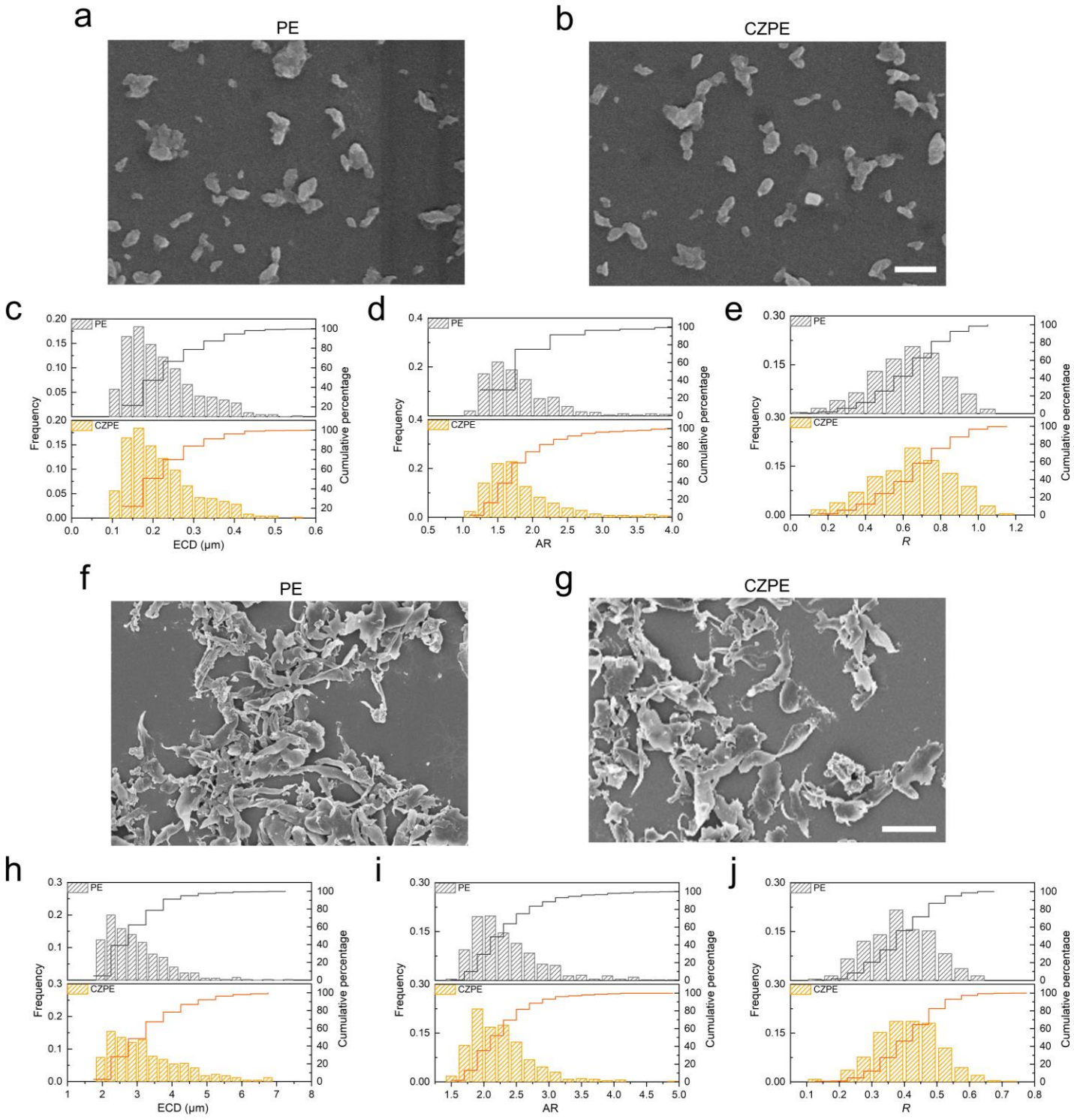

Supplementary Fig. ~~10~~11 | Size and morphology analysis of wear particles. Representative SEM images of smaller **a**, PE and **b**, CZPE particles, and corresponding **c**, ECD, **d**, AR, and **e**, R statistical analysis (n = 5, 100 particles per sample). Scale bar, 2 μm. Representative SEM images of larger **f**, PE and **g**, CZPE particles, and corresponding **h**, ECD, **i**, AR, and **j**, R statistical analysis (n = 5, 100 particles per sample). Scale bar, 10 μm. The summary of wear particle characteristics in supplementary table 2.

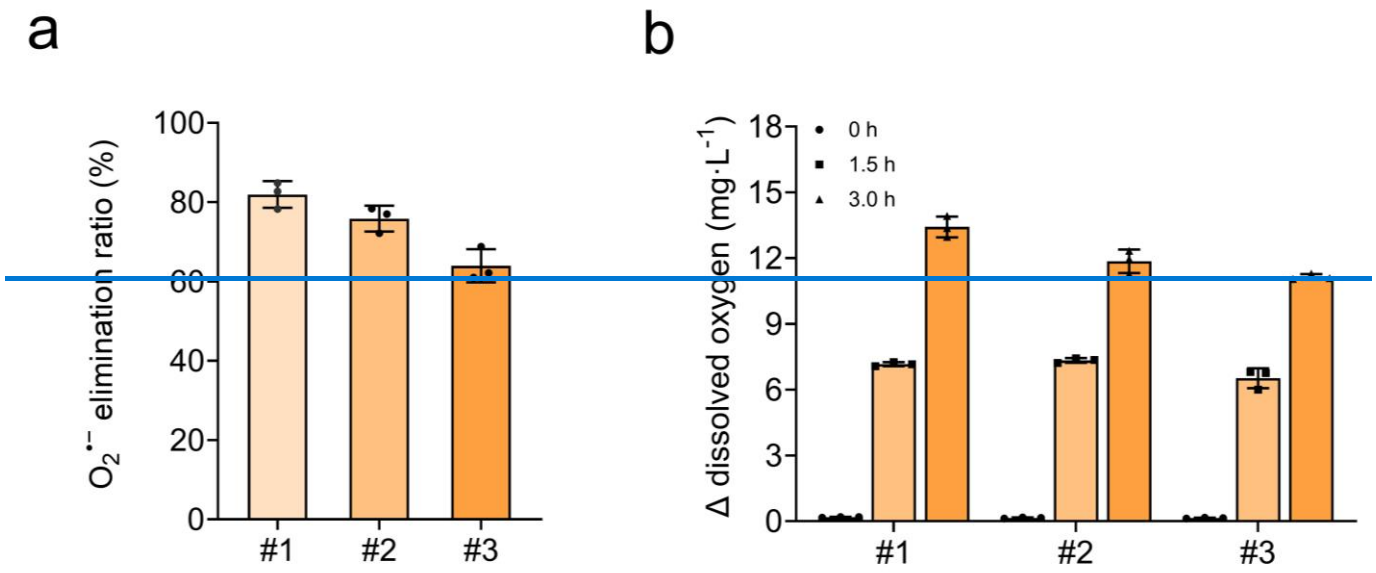

Supplementary Fig. 11 | Recycling stability of CZPE. a, $O_2^{\bullet-}$ elimination efficiency following two cycles of reuse ($n = 3$). **b**, Oxygen generation from H_2O_2 catalyzed by the CAT-like activity of CZPE at various time points, including after two cycles of reuse ($n = 3$). Data are presented as mean ± s.d.

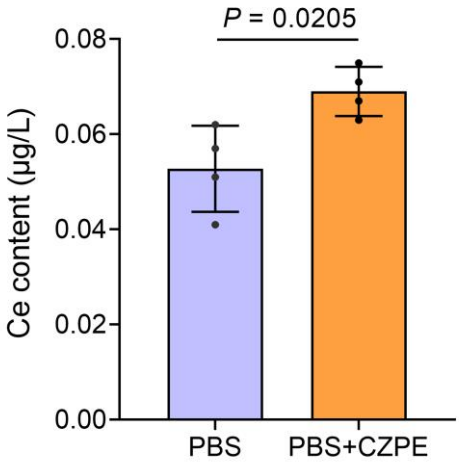

Supplementary Fig. 12 | Stability assessment of CZPE. Leakage of ~~cerium~~Ce ions after one-year immersion in PBS at room temperature. The ~~cerium~~Ce presence in the leachate was only 0.016 ppm of the total ~~cerium~~Ce content within CZPE in the immersion system (n = 4). Data are presented as mean ± s.d. P values were analysed by an unpaired t-test.

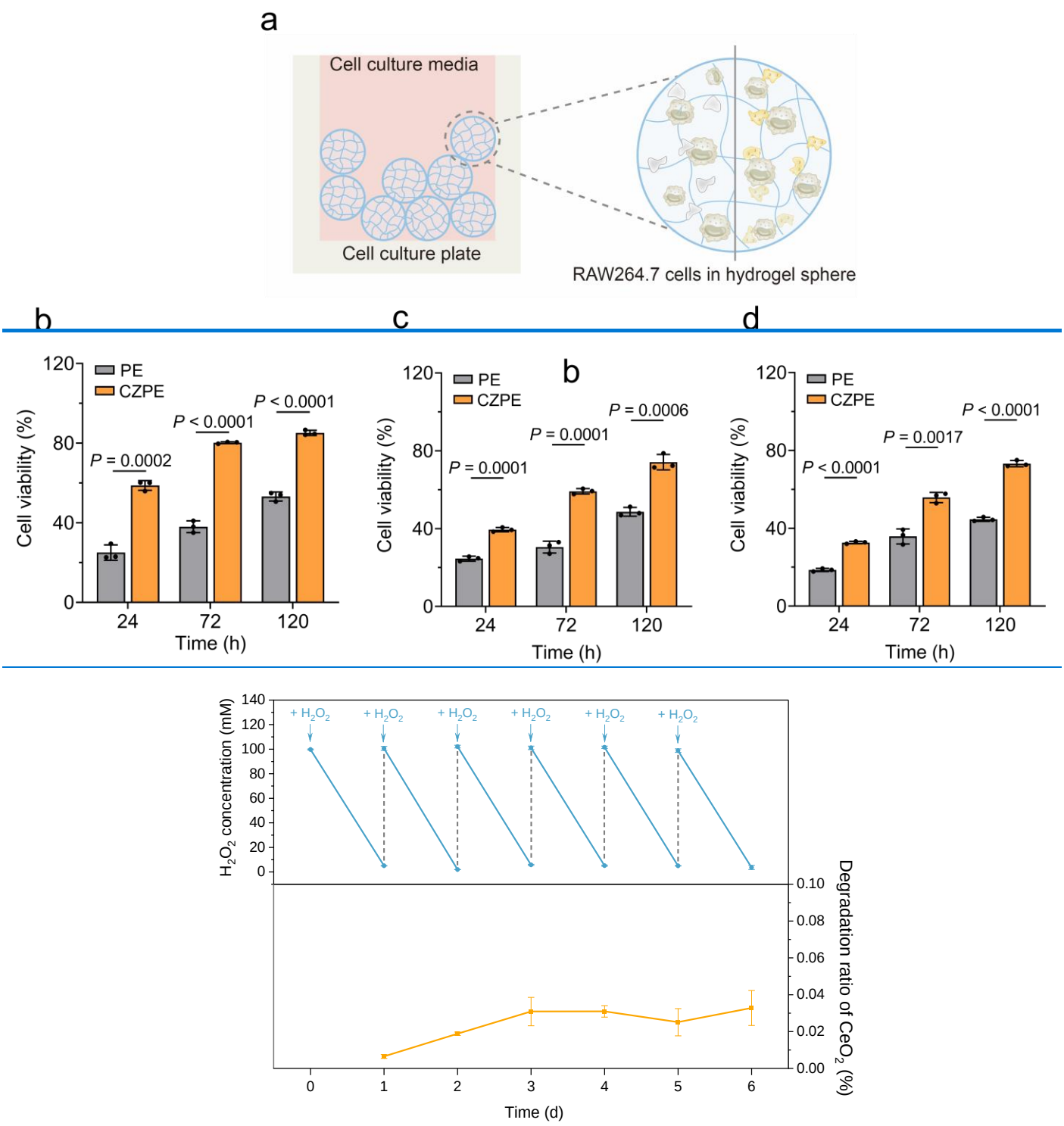

Supplementary Fig. 13 | Stability of CeO_2 in CZPE under oxidative conditions. Top: H_2O_2 concentration in the reaction system, monitored every 24 hours by measuring UV-vis absorbance at 240 nm[25] (n = 3). After each measurement, H_2O_2 was replenished to a concentration of 100 mM. Bottom: degradation ratio of CeO_2 in CZPE, calculated based on the concentration of Ce ions in the supernatant collected from the reaction system (n = 3). Data are presented as mean ± s.d.

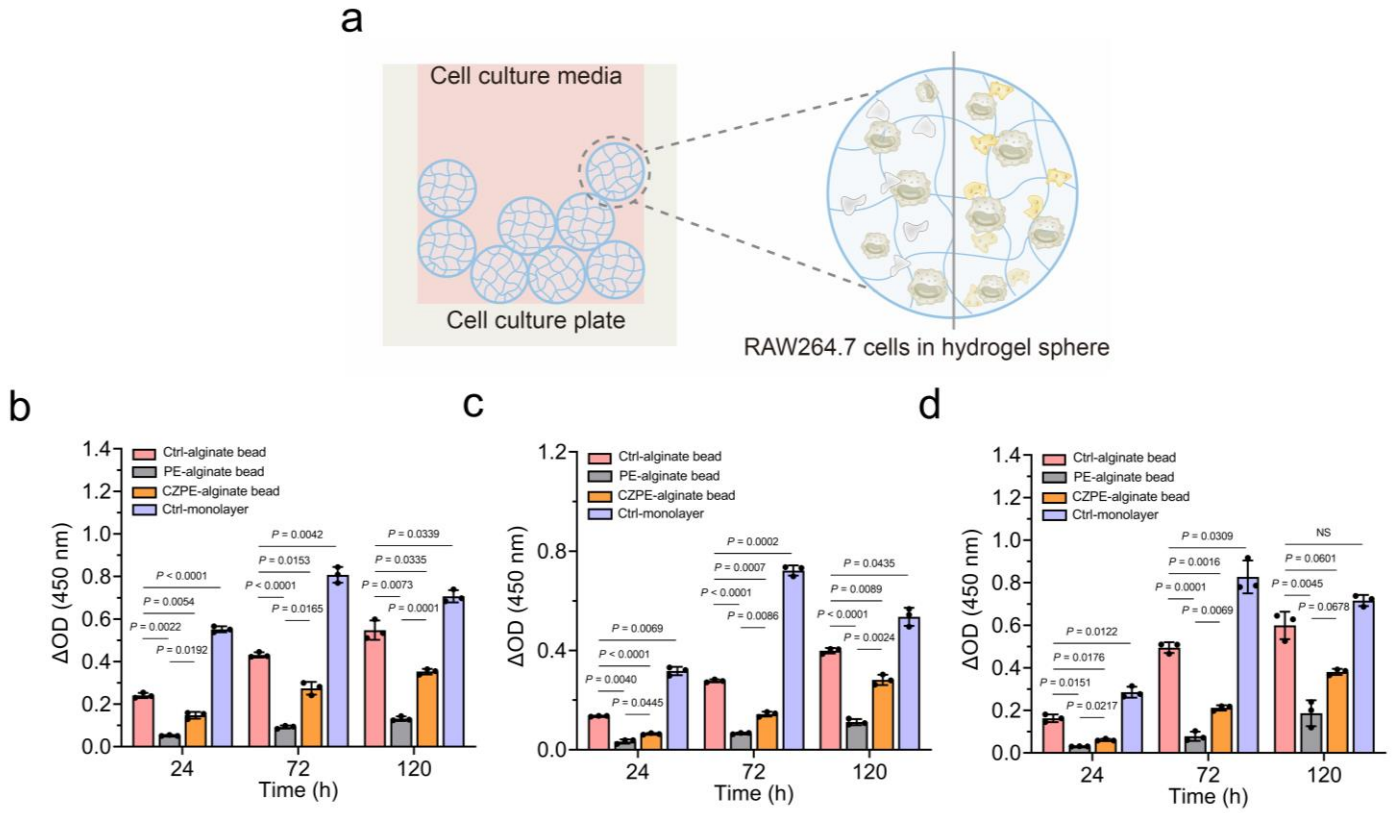

Supplementary Fig. 14 | Cytotoxicity evaluation of PE and CZPE-5 particles. Quantification of cell proliferation in 3D alginate beads and 2D/monolayer conditions using the CCK-8 assay. **a**, Schematic representation of the microsphere-cell interaction. ~~Cell viability of~~ΔOD values at 450 nm were measured for three different cell types, including **b**, RAW264.7 cells, **c**, MC3T3-E1 cells, and **d**, mouse synovial fibroblasts ~~post~~cultured in alginate microspheres or on standard cell culture plates for 24, 72, and 120~~-h incubation with PE and CZPE particles (n = 3). Data are presented as mean ± s.d. P values were analyzed by an unpaired t-test.~~ hours (n = 3). The Ctrl group represents cells cultured without particle stimulation. Data are presented as mean ± s.d. P values were analysed by ~~an unpaired t-test~~two-way ANOVA with Tukey's multiple comparisons test. NS, not significant, $P \geq 0.05$.

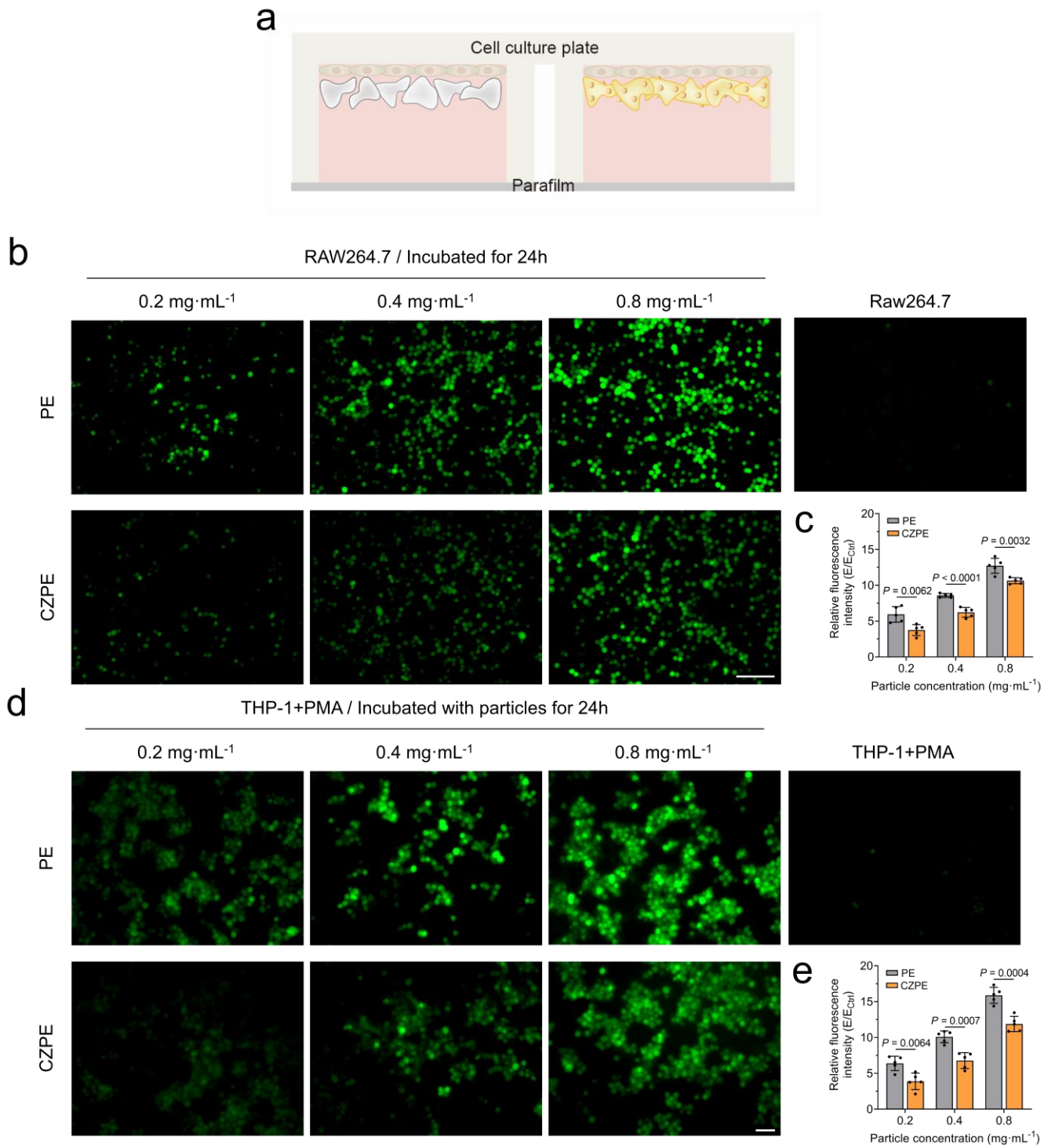

Supplementary Fig. ~~14~~15 | Assessment of ROS production induced by PE and CZPE-5 particles. a, Schematic of the inverted cell model for the assay. **b**, Representative fluorescence microscopy images depicting ROS levels in RAW264.7 cells post 24-h incubation with PE and CZPE-5 particles. Scale bar: 100 μm **c**, Quantitative analysis of fluorescence intensity corresponding to ROS levels from **b** (n = 5). **d**, Representative fluorescence microscopy images depicting ROS levels in macrophage-like phenotype THP-1 cells post 24-h incubation with PE and CZPE-5 particles. Scale bar, 50μm. **e**, Corresponding quantitative analysis of fluorescence intensity correlating to ROS levels from **d** (n = 5). Data are presented as mean ± s.d. P values were analysed by an unpaired t-test.

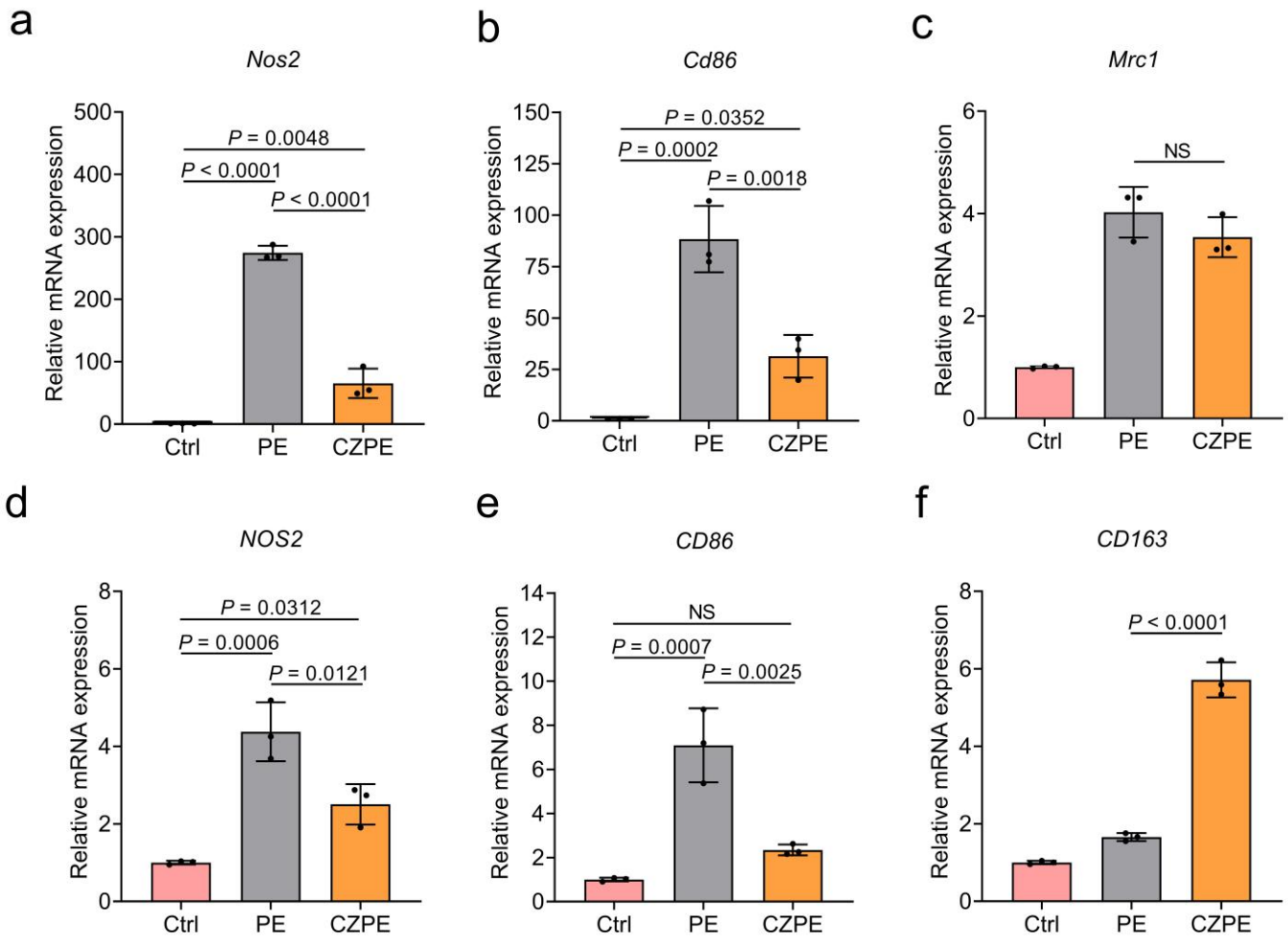

Supplementary Fig. ~~15~~16 | Relative mRNA expression levels of macrophage polarization markers measured by qRT-PCR. a, *Nos2* (encodes iNOS2, marker of M1 macrophage), **b**, *Cd86* (encode CD86, marker of M1 macrophage), and **c**, *Mrc1*(encode CD206, marker of M2 macrophage) in RAW264.7 cells stimulated by wear particles (n = 3). **d,** *NOS2* (encodes iNOS2, marker of M1 macrophage), **e**, *CD86* (encode CD86, marker of M1 macrophage), and **f**, *CD163* (encode CD163, marker of M2 macrophage) in THP-1-derived macrophages stimulated by wear particles (n = 3). Data are presented as mean ± s.d. P values were ~~analyzed~~analysed by one-way ANOVA with Tukey's multiple comparisons test.

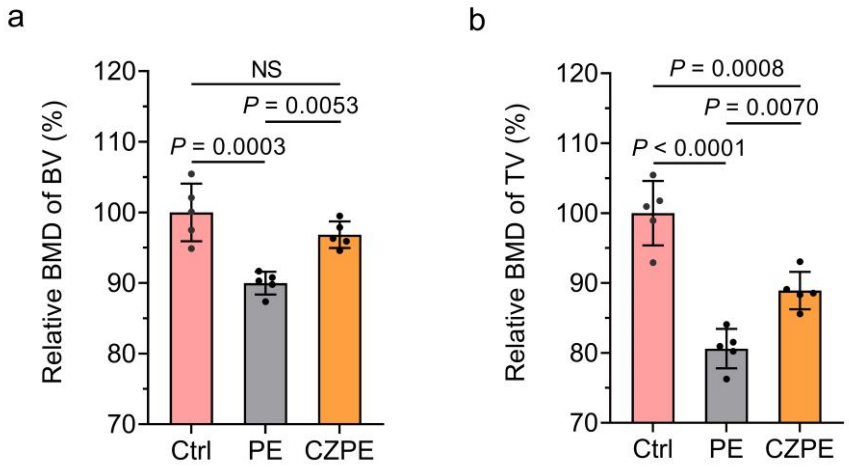

Supplementary Fig. ~~16~~17 | Statistical analysis of bone parameters in a particle-induced cranial bone resorption model. a, Relative BMD of BV. **b**, Relative BMD of TV (n = 5). Data are presented as mean ± s.d. P values were analysed by one-way ANOVA with Tukey's multiple comparisons test. NS, not significant, $P \geq 0.05$.

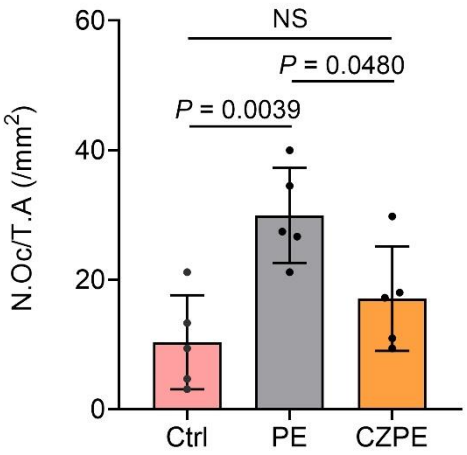

Supplementary Fig. ~~17~~18 | Quantification of osteoclast density in TRAP-stained sections of cranial bones (*n* = 5). Data are presented as mean ± s.d. *P* values were analysed by one-way ANOVA with Tukey's multiple comparisons test. NS, not significant, $P \geq 0.05$.

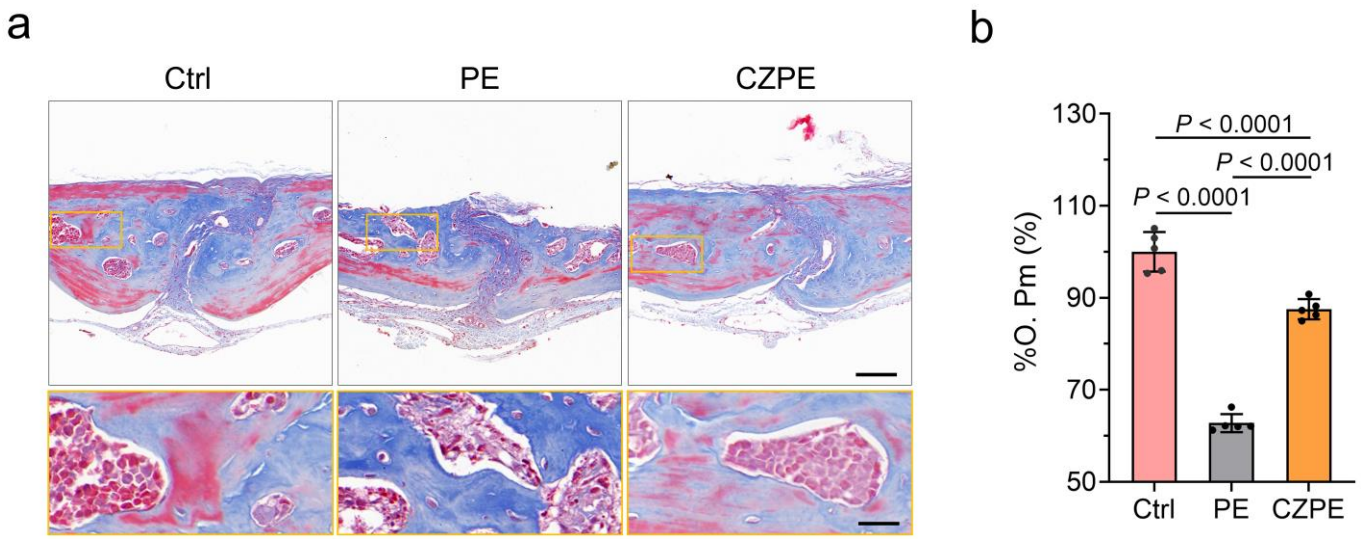

Supplementary Fig. ~~18~~19 | Influence of PE and CZPE-5 particles on osteogenic potential in calvarial bone tissue. a, Representative Masson's trichrome-stained bone sections at day 14 post-injection, showing collagen deposition (blue) and mineralized bone (red). Images depict top: 20× magnification, scale bar, 100 µm; bottom: 80× magnification, scale bar, 20 µm. **b**, Quantitative analysis of the %O. Pm (n = 5). Data are presented as mean ± s.d. P values were analysed by one-way ANOVA with Tukey's multiple comparisons test.

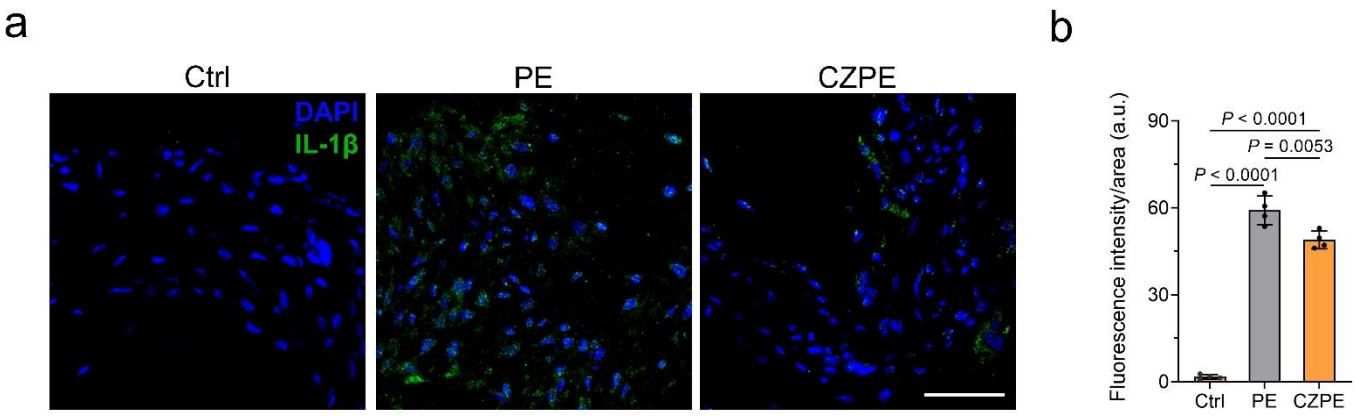

Supplementary Fig. ~~19~~20 | Inflammatory response in calvarial bones induced by PE and CZPE-5 particles. **a**, Representative immunofluorescence images of calvarial sections at day 14 post-injection. IL-1β is marked in green, and nuclei are stained with DAPI in blue. Scale bar, 40 μm. **b**, Quantitative evaluation of IL-1β fluorescence intensity (n = 4). Data are presented as mean ± s.d. P values were analysed by one-way ANOVA with Tukey's multiple comparisons test.

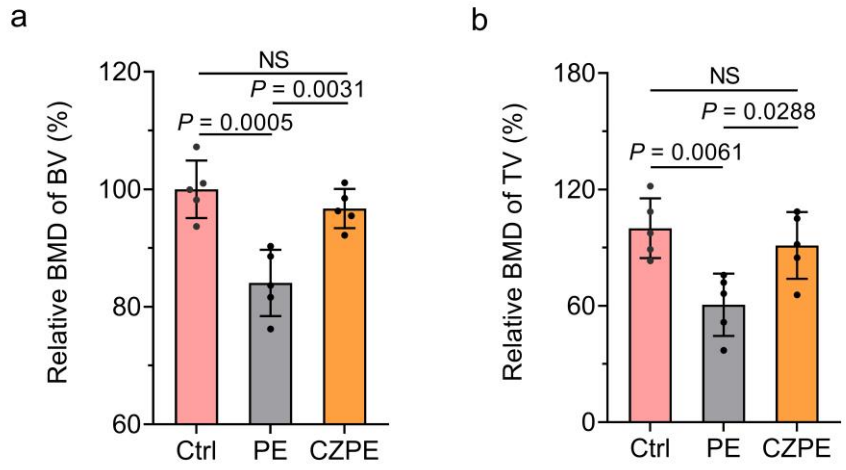

Supplementary Fig. ~~20~~21 | Bone parameter statistics for distal femoral implant models. a, Relative BMD of BV. **b**, Relative BMD of TV (n = 5). Data are presented as mean ± s.d. P values were analysed by one-way ANOVA with Tukey's multiple comparisons test. NS, not significant, $P \geq 0.05$.

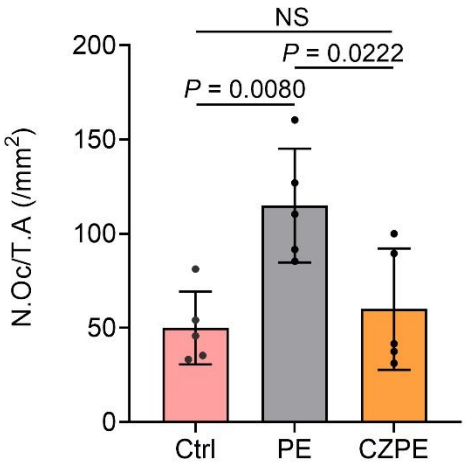

Supplementary Fig. ~~21~~22 | Osteoclast density statistics in TRAP-stained femur sections (*n* = 5). Data are presented as mean ± s.d. *P* values were analysed by one-way ANOVA with Tukey's multiple comparisons test. NS, not significant, $P \geq 0.05$.

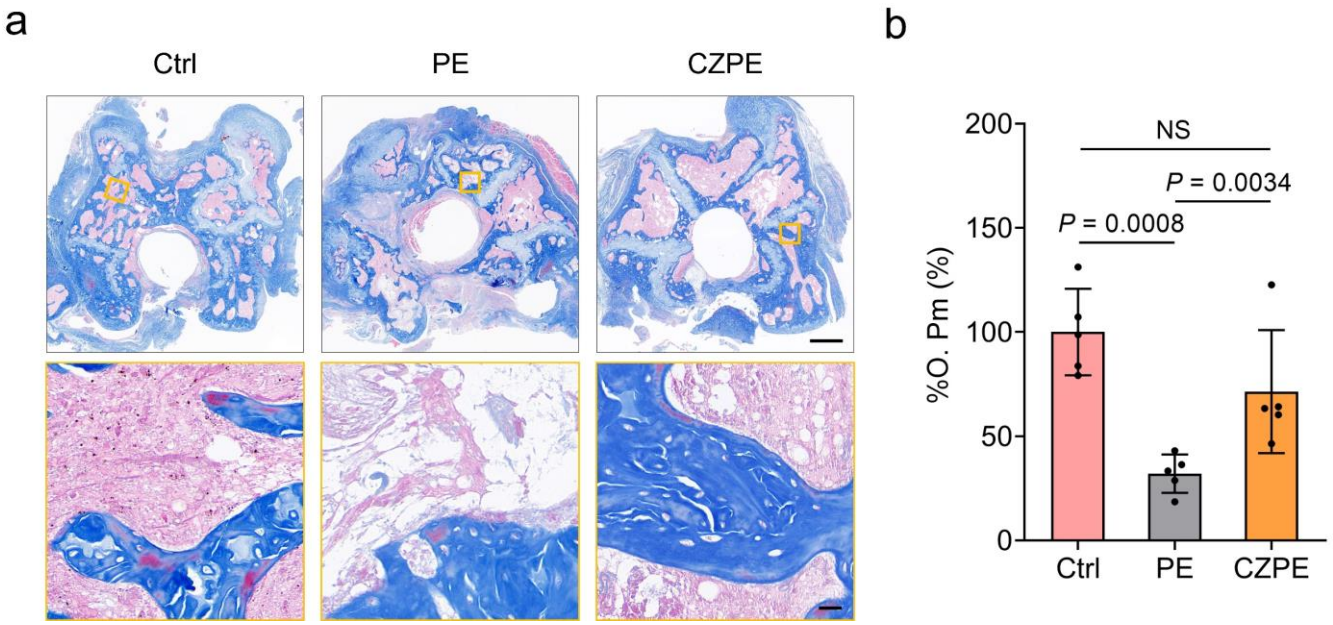

Supplementary Fig. ~~22~~23 | Influence of PE and CZPE-5 particles on osteogenic potential in femoral bone tissue. a, Representative Masson's trichrome-stained bone sections at day 49 post-injection, showing collagen deposition (blue) and mineralized bone (red). Images depict top: 3× magnification, scale bar, 500 µm; bottom: 48× magnification, scale bar, 20 µm. **b**, Quantitative analysis of the %O. Pm (n = 5). Data are presented as mean ± s.d. P values were analysed by one-way ANOVA with Tukey's multiple comparisons test. NS, not significant, $P \geq 0.05$.

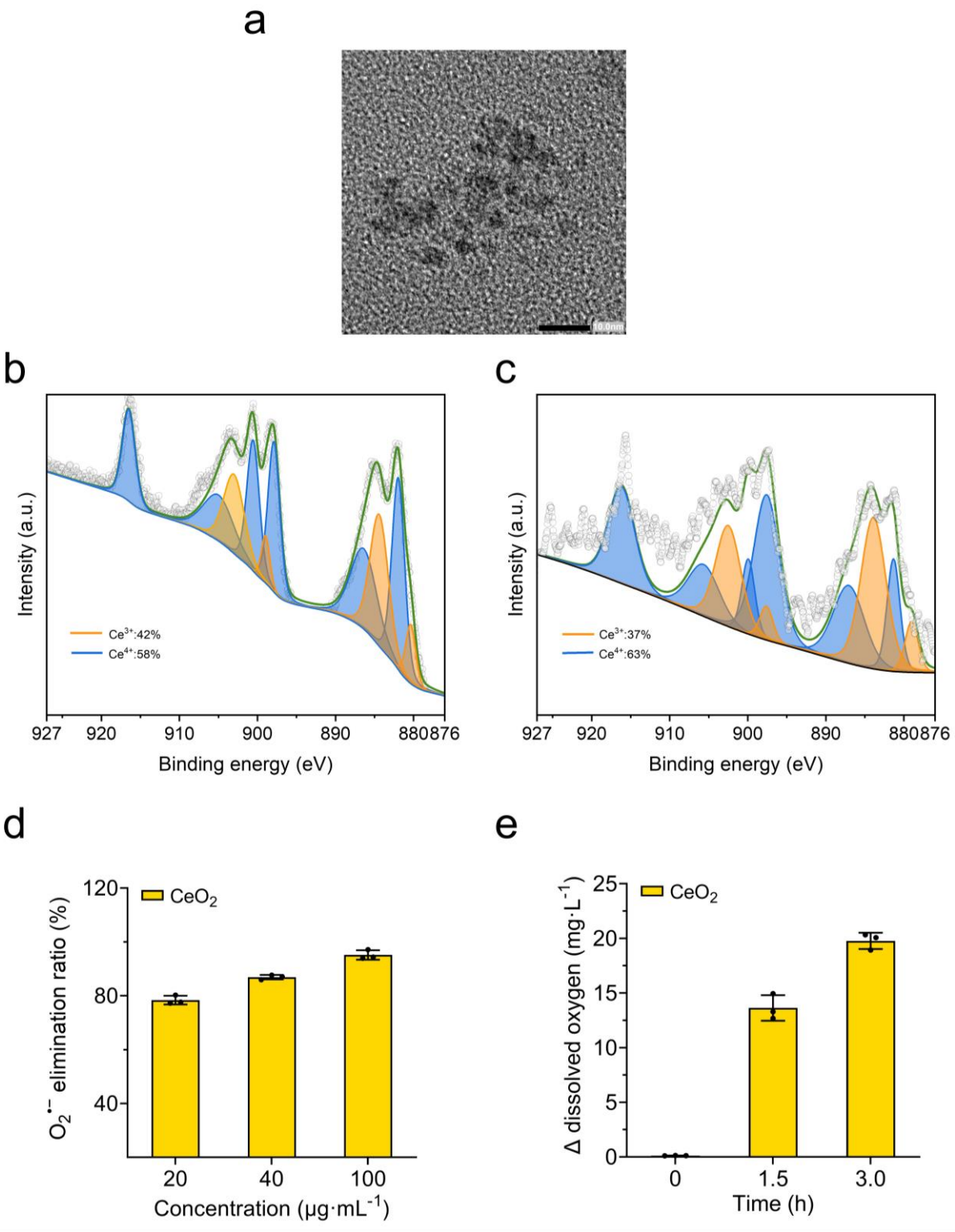

Supplementary Fig. ~~23~~24 | Characterization of CeO_2 NPs and CZPE particles. Representative TEM image of **a**, CeO_2 NPs. XPS spectra of Ce 3*d* in **b**, CeO_2 NPs and **c**, CeO_2 within CZPE particles. Antioxidative activity assays of CeO_2 NPs: SOD-like activity (**d**) and CAT-like activity (**e**) ($n = 3$). Data are presented as mean ± s.d. ~~*P* values were analyzed by an unpaired t-test. NS, not significant, $P \geq 0.05$.~~

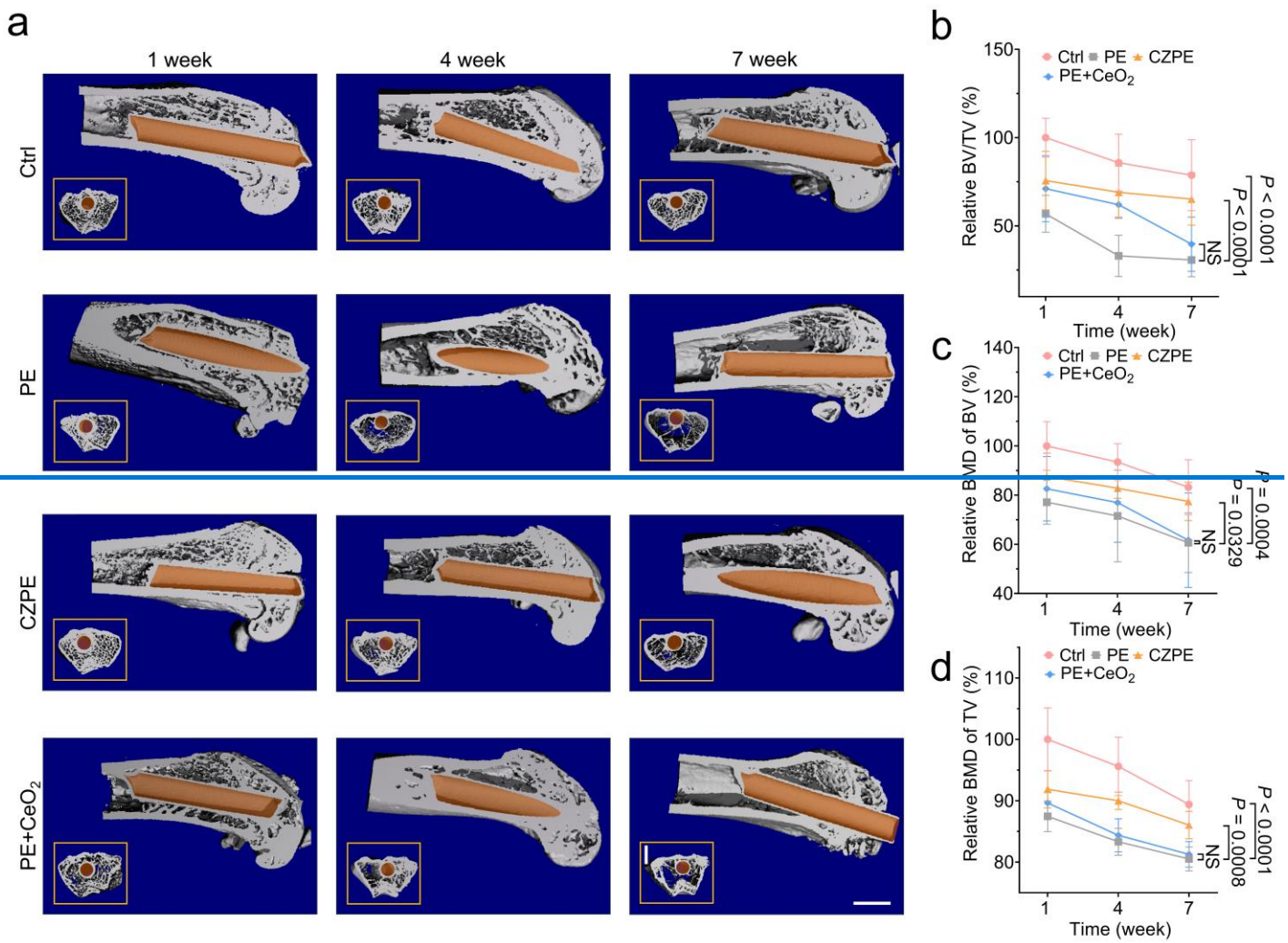
a
1 week
4 week
7 week
Ctrl
PE
CZPE
PE+CeO2
b
Ctrl PE CZPE
PE+CeO2
Relative BV/TV (%)
150
100
50
P < 0.0001
P < 0.0001
NS
1
4
7
Time (week)
c
Ctrl PE CZPE
PE+CeO2
Relative BMD of BV (%)
140
120
100
80
60
40
P = 0.0004
P = 0.0329
NS
1
4
7
Time (week)
d
Ctrl PE CZPE
PE+CeO2
Relative BMD of TV (%)
110
100
90
80
P < 0.0001
P = 0.0008
NS
1
4
7
Time (week)

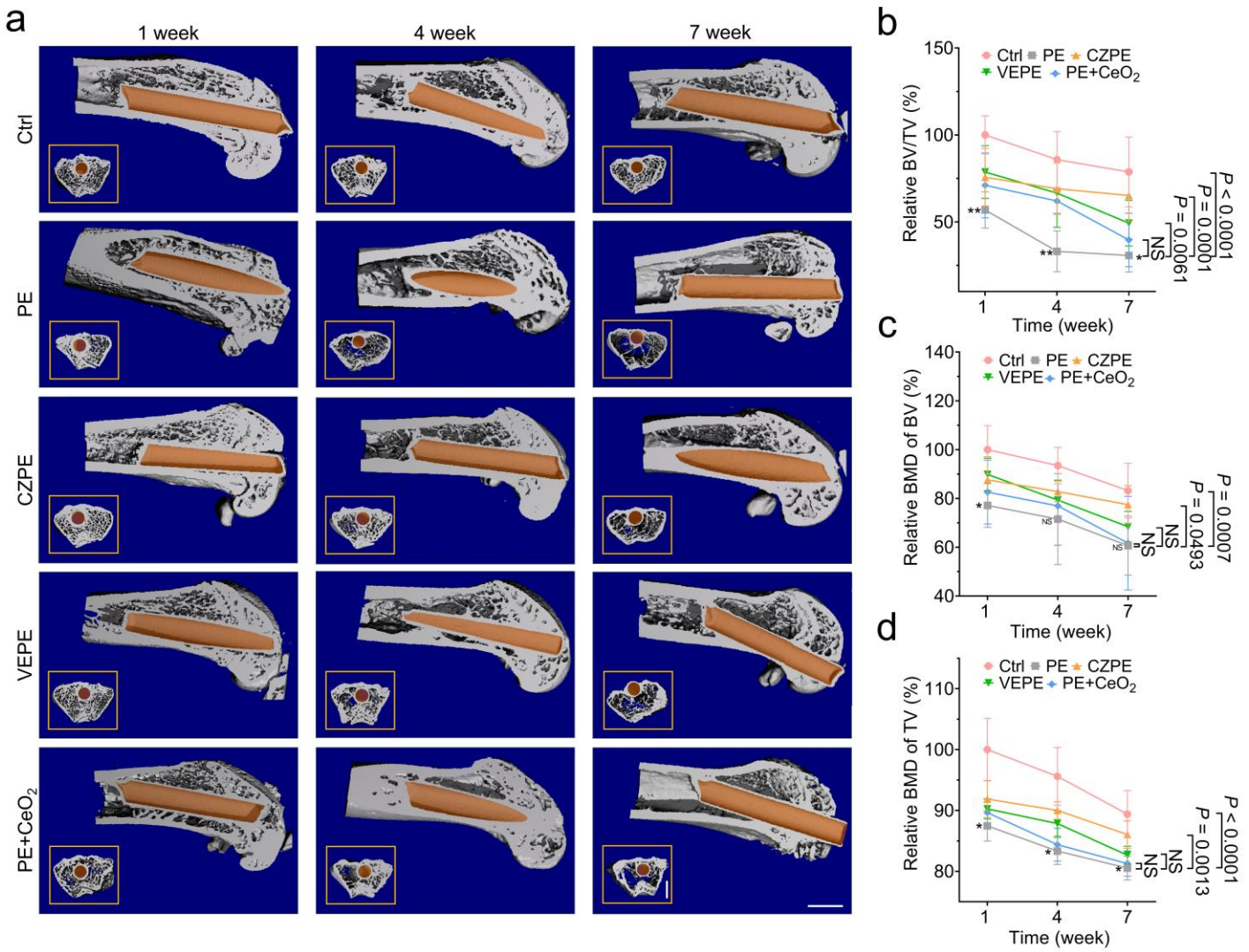

Supplementary Fig. ~~24~~25 | Bone resorption in femoral distal implant model at different time points. a, Representative micro-CT images of the femoral transverse section at weeks 1, 4, and 7 post-injection. Main images: femoral cross-section parallel to the direction of nail insertion. Insets: femoral cross-section perpendicular to the direction of nail insertion. Scale bar, 1 mm. Quantifications of relative **b**, BV/TV, **c**, BMD of BV, and **d**, BMD of TV corresponding to data in **a** (n = 5). Data are presented as mean ± s.d. P values were ~~analyzed~~analysed by two-way ANOVA with Tukey's multiple comparisons test. NS, not significant, $P \geqslant 0.05$.

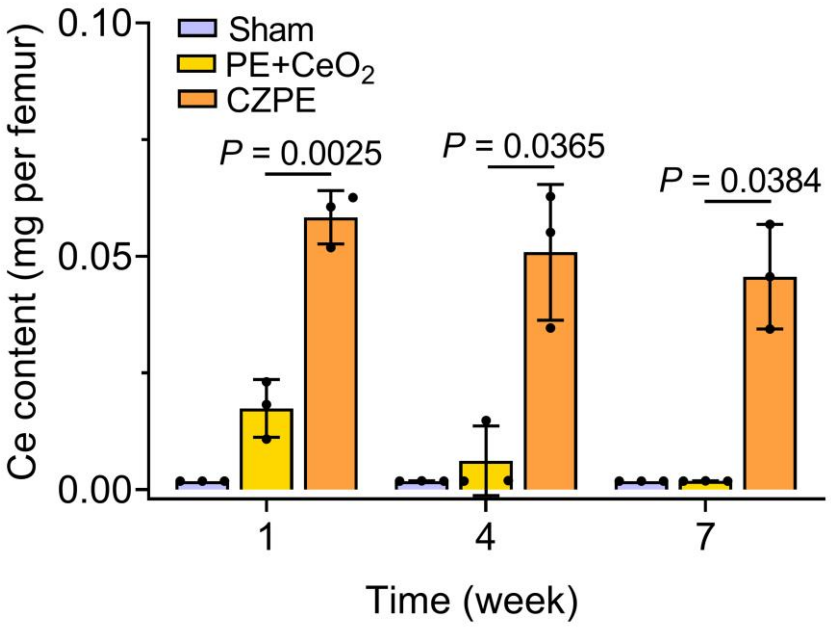

Supplementary Fig. ~~25~~26 | Ce content in mouse femurs at different time points (*n* = 3). Data are presented as mean ± s.d. *P* values were ~~analyzed~~analysed by two-way ANOVA with Tukey's multiple comparisons test. NS, not significant, *P* ~~>~~ ≥ 0.05.

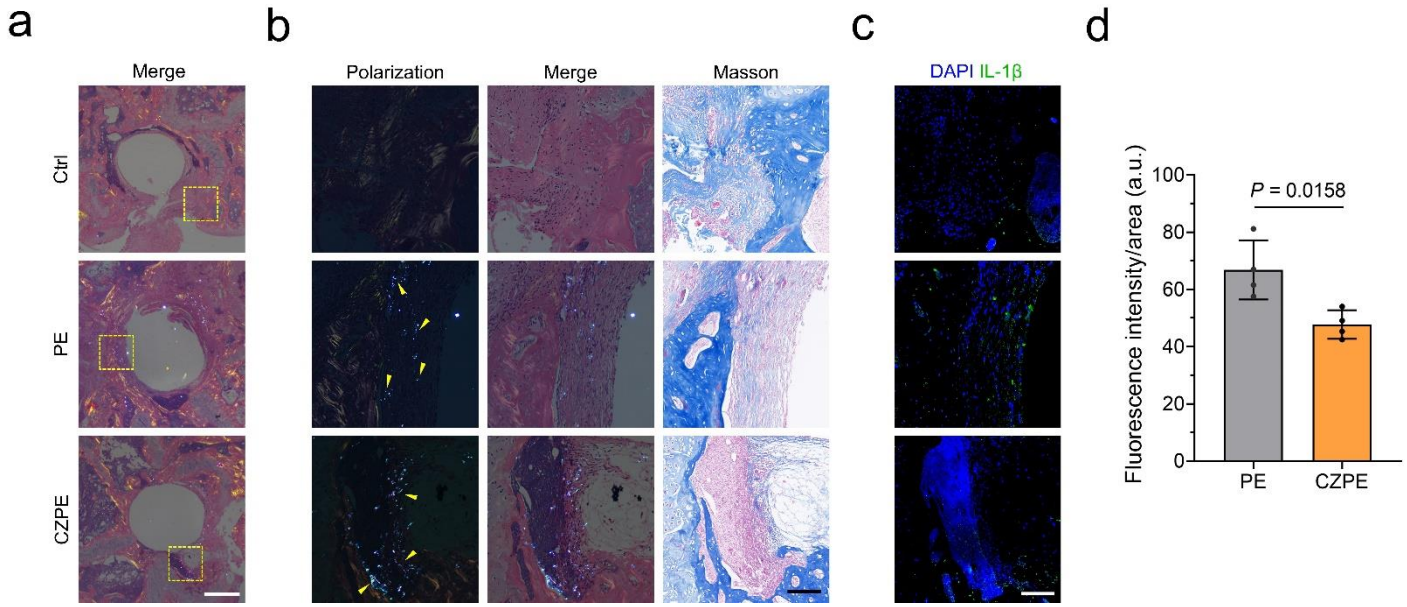

Supplementary Fig. ~~26~~27 | Intramedullary distribution and inflammatory stimulation by PE and CZPE-5 particles in femoral bones. a, Representative overlaid images of polarized light microscopy and H&E staining of femur sections. Scale bar 500 μm. **b**, Enlarged views of the yellow dashed boxed areas in **a**, showing left: polarized light microscopy, yellow arrows indicate the presence of particles; center: combined polarized light and H&E staining; right: Masson's trichrome-staining. Scale bar 100 μm. **c**, IL-1β immunofluorescence staining. Green: IL-1β, blue: DAPI; Scale bar 100 μm. **d**, Quantification of IL-1β intensity in particle deposition areas (n = 4). Data are presented as mean ± s.d. P values were analysed by an unpaired t-test.

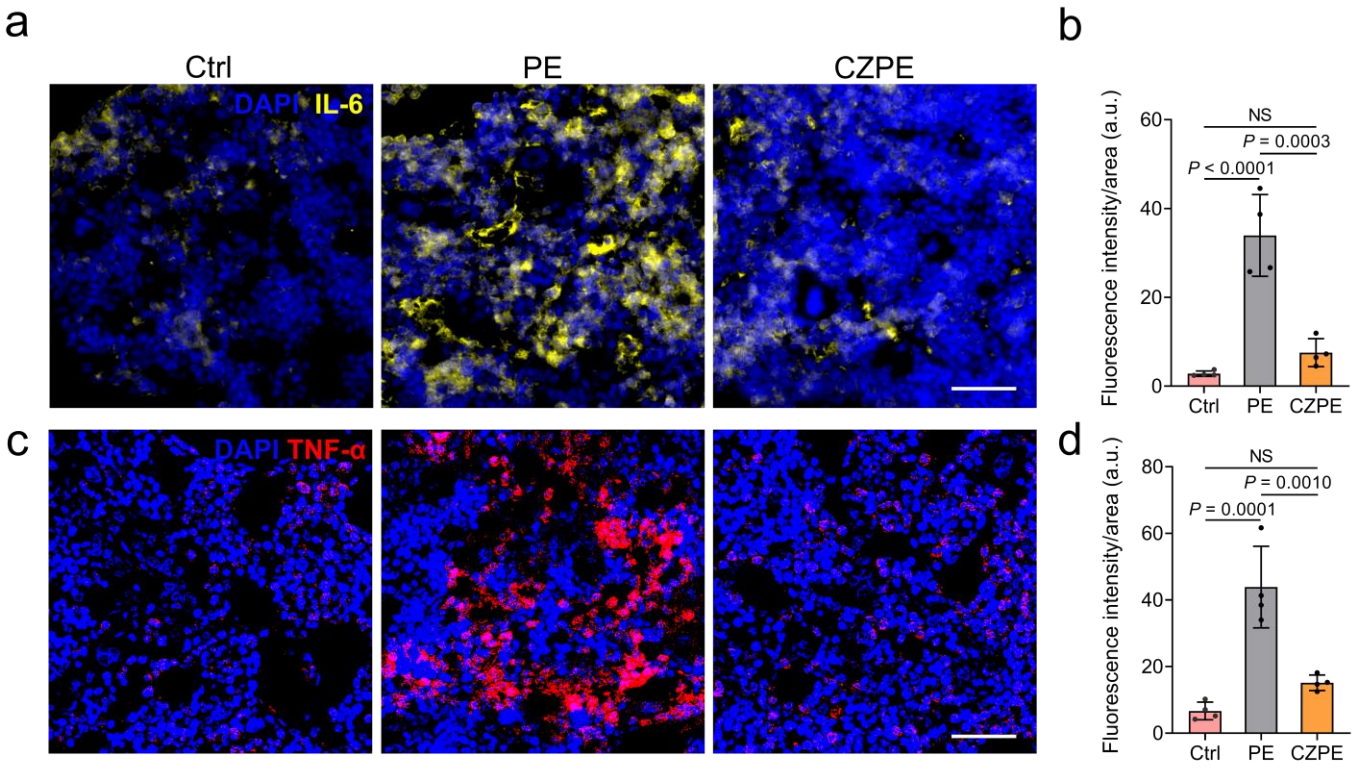

Supplementary Fig. ~~27~~28 | Inflammatory cytokine expression in the femoral marrow medulla. a, Representative immunofluorescence images for DAPI and IL-6 co-staining. Scale bar, 20 μm. IL-6 is marked in yellow, and nuclei are stained with DAPI in blue. **b**, Quantitative evaluation of IL-6 fluorescence intensity (n = 4). **c**, Representative immunofluorescence images for DAPI and TNF-α co-staining. Scale bar, 20 μm. TNF-α is marked in red, and nuclei are stained with DAPI in blue. **d**, Quantitative evaluation of TNF-α fluorescence intensity (n = 4). Data are presented as mean ± s.d. P values were analysed by one-way ANOVA with Tukey's multiple comparisons test. NS, not significant, $P \geq 0.05$.

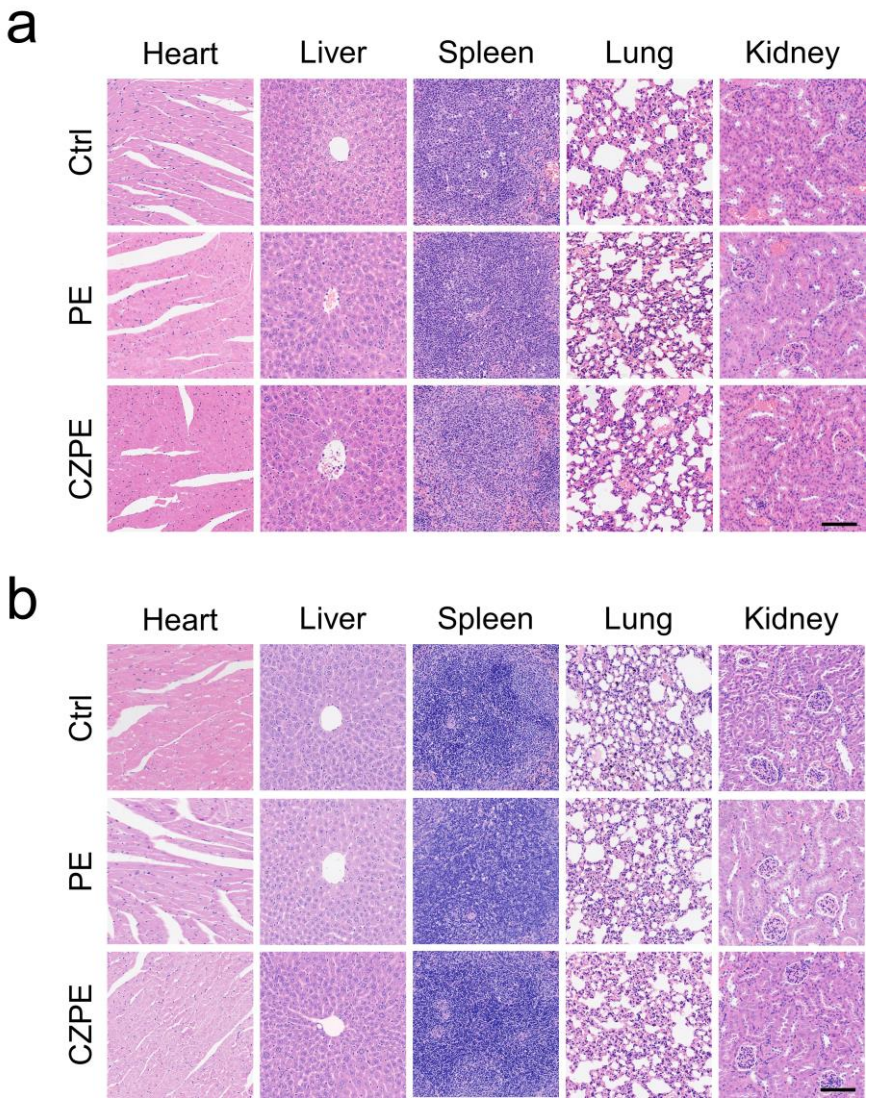

Supplementary Fig. ~~28~~29 | Histological analysis with H&E staining of major organ sections from experimental animals. a, Calvaria osteolysis model. **b**, Distal femur implant model. Scale bars, 100 μm. Experiments were independently repeated thrice with similar results in different animals.

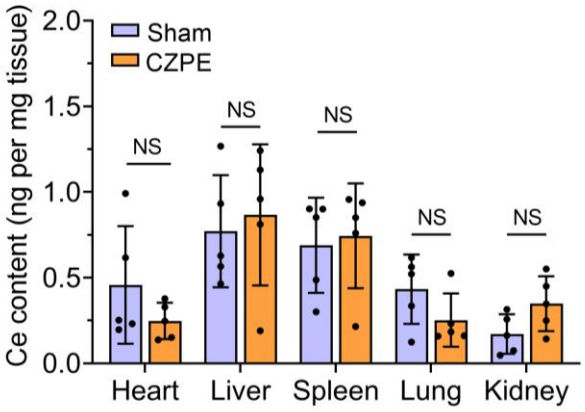

Supplementary Fig. ~~29 | Cerium~~30 | Ce content in major organs of mice implanted with CZPE particles versus sham mice. Analysis of ~~cerium~~Ce content in major organs (heart, liver, spleen, lung, and kidney) ($n = 5$). Data are presented as mean ± s.d. P values were analysed by an unpaired t-test. NS, not significant, $P \geqslant 0.05$.

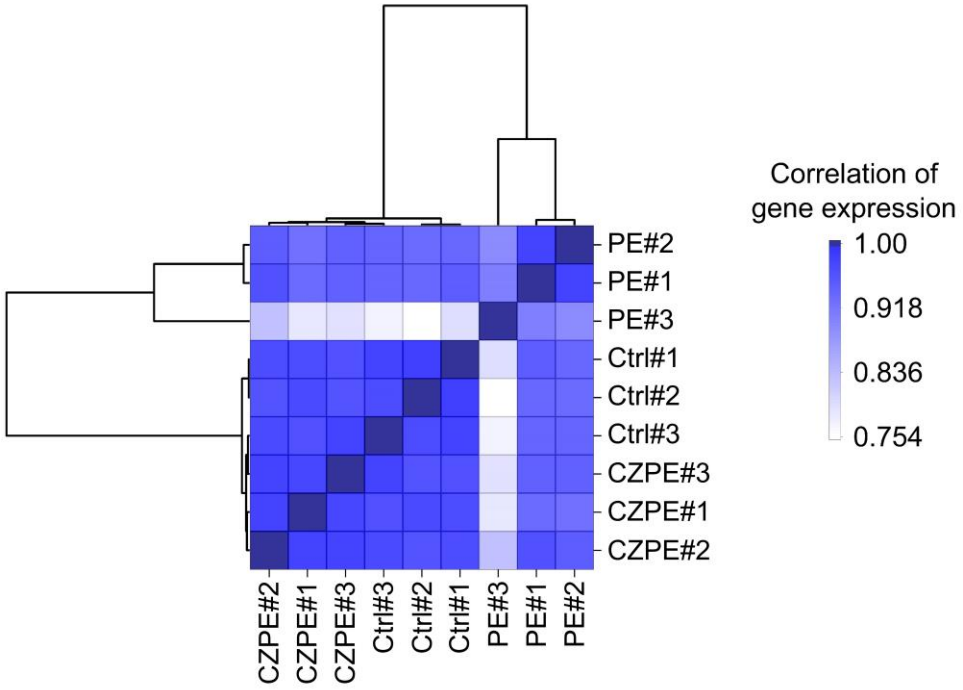

Supplementary Fig. ~~30~~31 | Pearson correlation heatmap of transcriptome sequencing data in distal femoral implant model mice. Heatmap clustering was performed using the Ward clustering algorithm (n = 3).

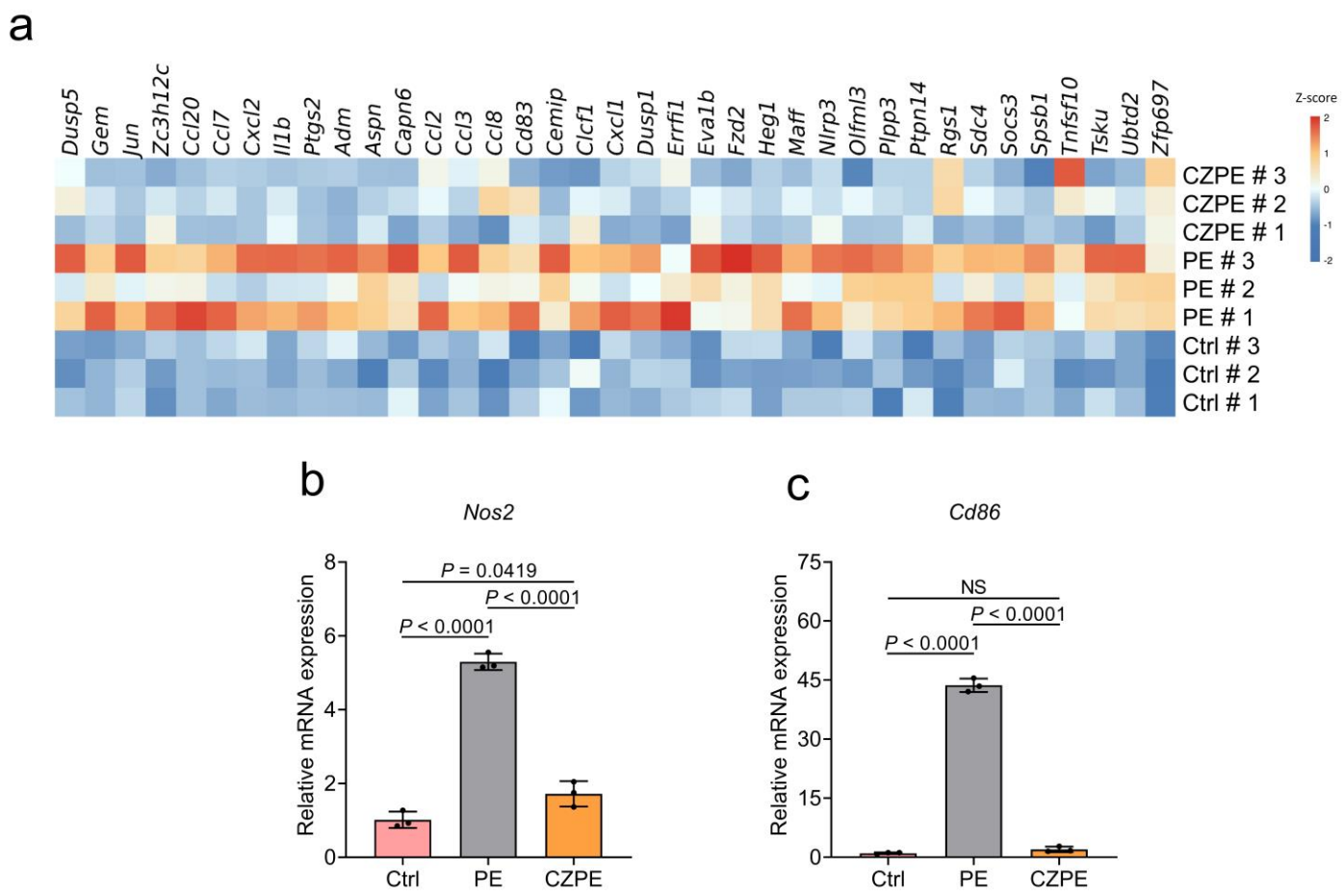

Supplementary Fig. ~~31~~32 | Expression of genes associated with macrophage polarization in mouse femurs. **a**, Heatmap displaying the expression levels of genes highly expressed by M1 macrophages during foreign body reactions[14~~26~~]. All genes displayed are differentially expressed genes (DEGs) (n = 3). Relative mRNA expression levels of **b**, *Nos2*, and **c**, *Cd86* in femur tissues (n = 3). Data are presented as mean ± s.d. P values were ~~analyzed~~analysed by one-way ANOVA with Tukey's multiple comparisons test. NS, not significant, $P \geq 0.05$.

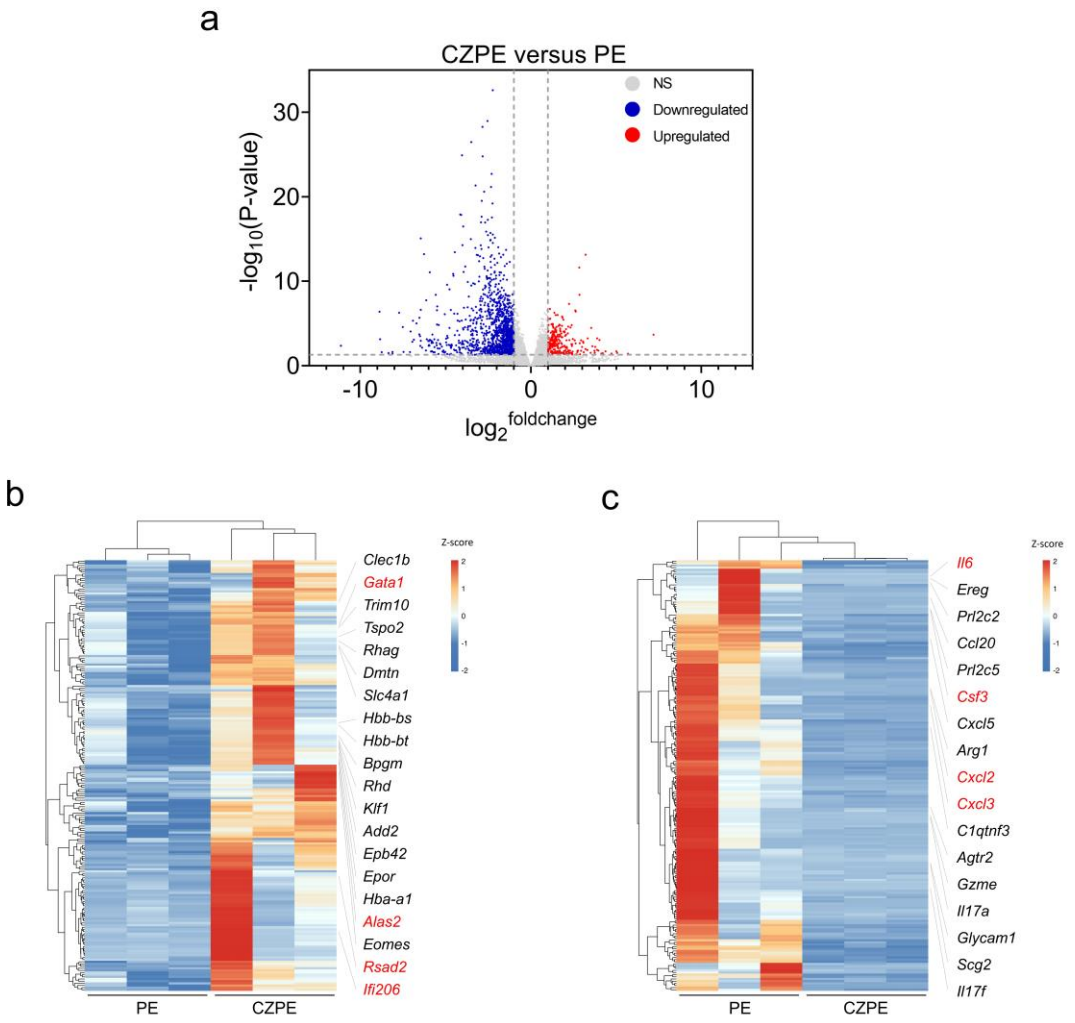

Supplementary Fig. ~~32~~33 | Differential gene expression analysis between CZPE and PE Groups. a, Volcano plot of genes differentially expressed (upregulated: $P < 0.05$, $\log_2^{\text{foldchange}} > 1$; downregulated: $P < 0.05$, $\log_2^{\text{foldchange}} < -1$) between CZPE and PE clusters. **b**, Heatmap illustrating the expression of the top 200 genes upregulated in the CZPE group compared to the PE group, with highlighted genes associated with hematopoietic functions. **c,** Heatmap displaying the top 200 downregulated genes in the CZPE group compared to the PE group, with highlighted genes associated with inflammatory response ($n = 3$).

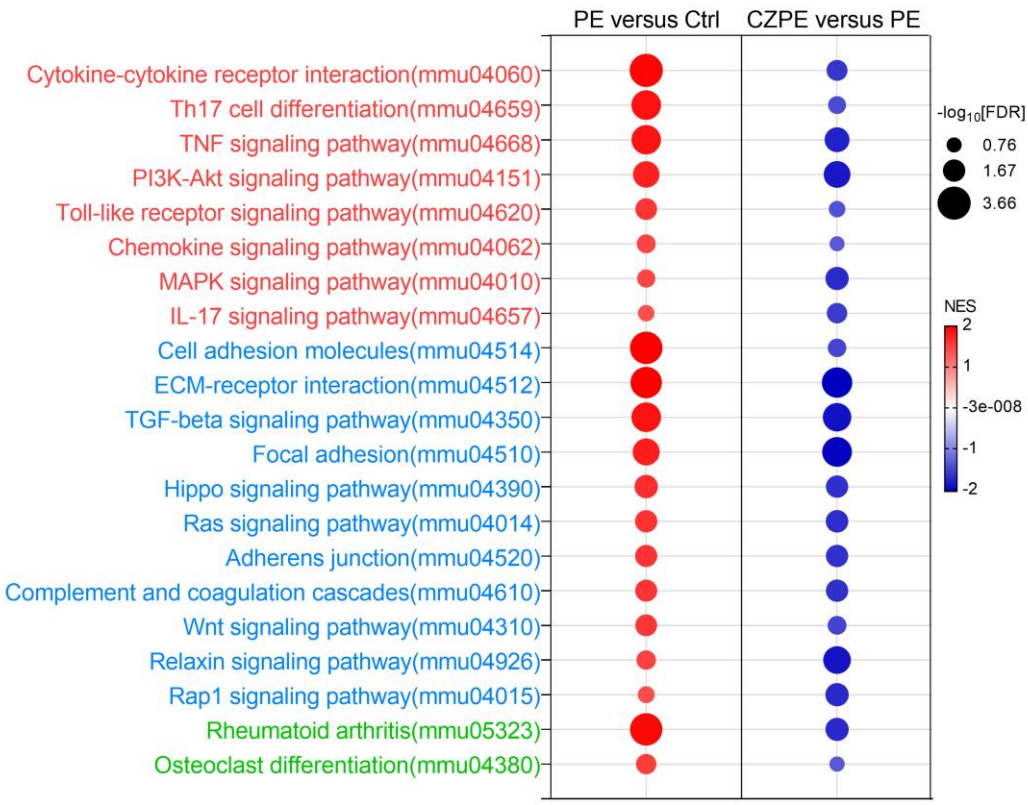

Supplementary Fig. ~~33~~34 | GSEA (P < 0.05; FDR < 0.25) of WPO-related pathways. Pathways mmu04060 through mmu04657 pertain to inflammation-related signaling (red), mmu04514 to mmu04015 to foreign body reaction signaling (blue), and mmu05323 and mmu04380 to osteoclast differentiation signaling (green).

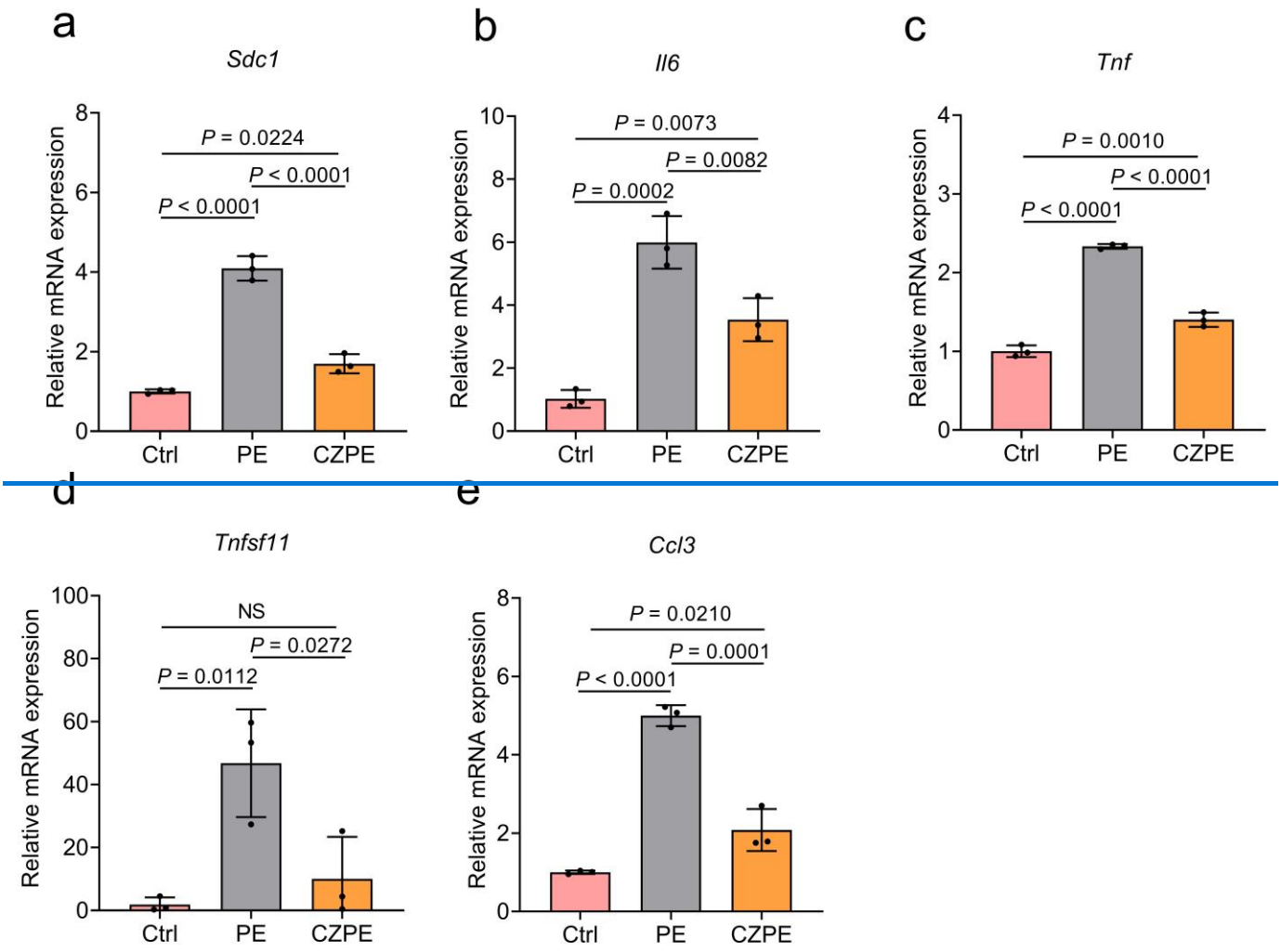
a
Sdc1
Relative mRNA expression
P = 0.0224
P < 0.0001
P < 0.0001
Ctrl
PE
CZPE
b
Il6
Relative mRNA expression
P = 0.0073
P = 0.0082
P = 0.0002
Ctrl
PE
CZPE
c
Tnf
Relative mRNA expression
P = 0.0010
P < 0.0001
P < 0.0001
Ctrl
PE
CZPE
d
Tnfsf11
Relative mRNA expression
NS
P = 0.0272
P = 0.0112
Ctrl
PE
CZPE
e
Ccl3
Relative mRNA expression
P = 0.0210
P = 0.0001
P < 0.0001
Ctrl
PE
CZPE

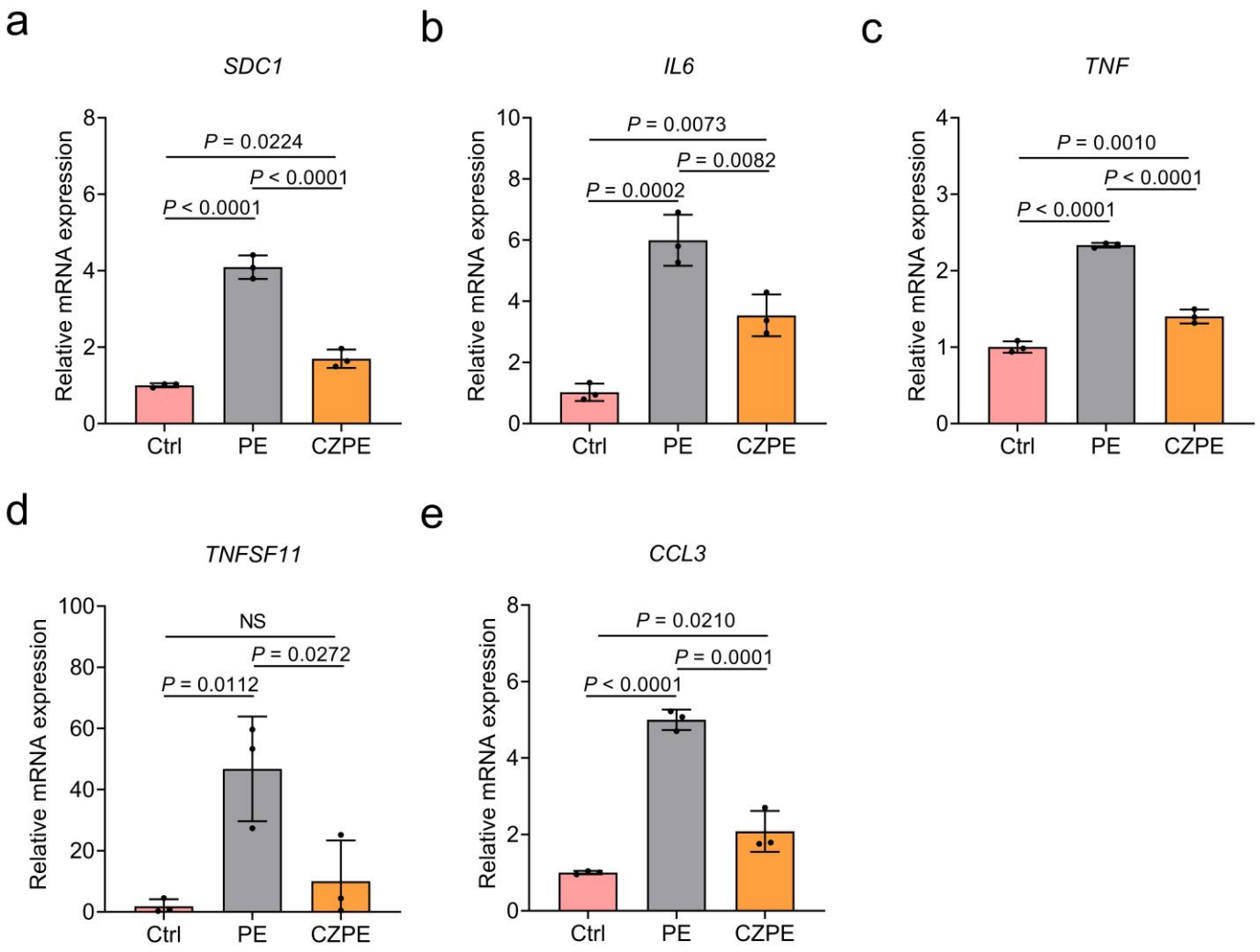

Supplementary Fig. ~~34~~35 | Relative mRNA expression levels of plasma markers and cytokines in U266B1 cells under an inflammatory environment. QRT-PCR analysis of relative mRNA expression of **a**, ~~*Sdc1*~~*SDC1*, **b**, ~~*Il6*~~*IL6*, **c**, ~~*Tnf*~~*TNF*, **d**, ~~*Tnfsf11*~~*TNFSF11* (encodes receptor activator of nuclear factor kappa-B ligand), and **e**, ~~*Ccl3*~~*CCL3* (encodes C-C motif chemokine 3) in U266B1 cells stimulated by supernatants from particles-stimulated RAW264.7 cells (n = 3). Data are presented as mean ± s.d. P values were ~~analyzed~~analysed by one-way ANOVA with Tukey's multiple comparisons test.

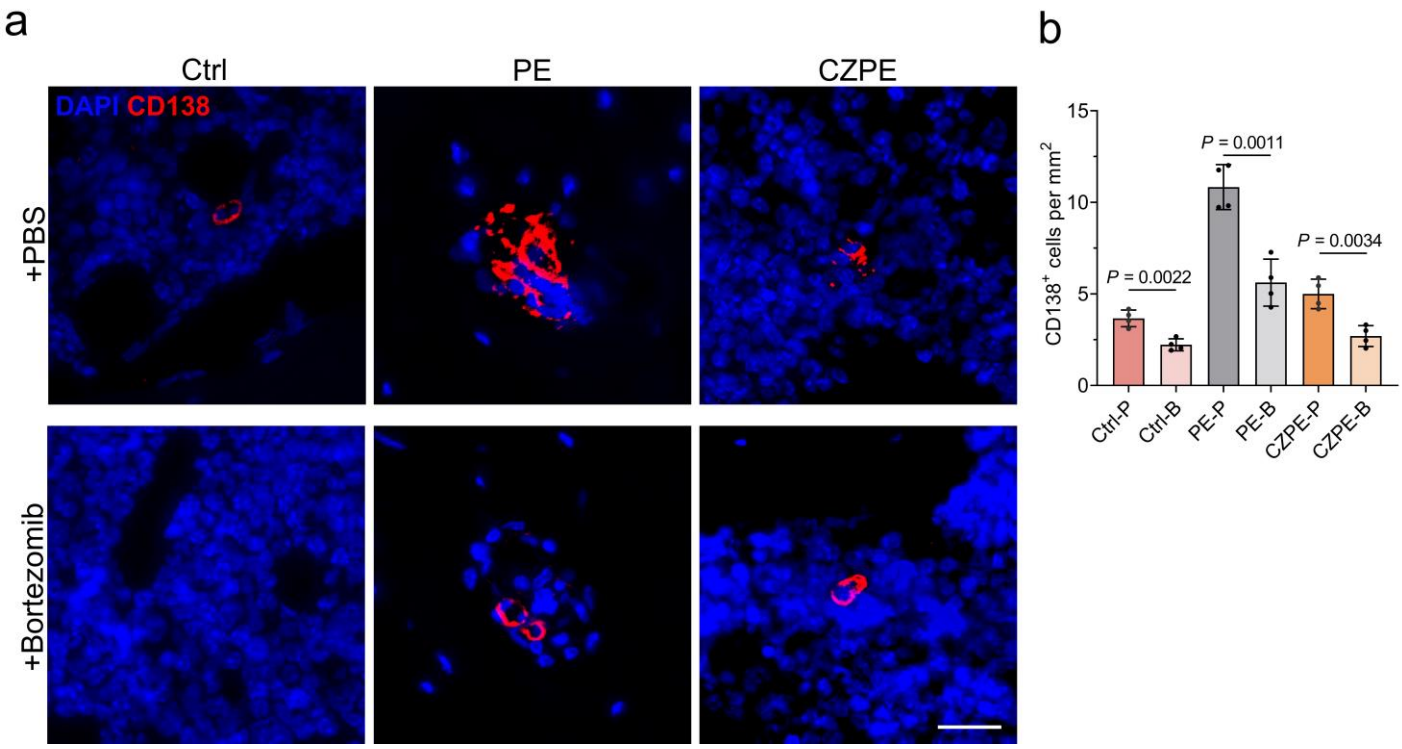

Supplementary Fig. ~~35~~36 | Depletion status of plasma cells around peri-implant areas after bortezomib treatment. a, Representative immunofluorescence images of femur sections after bortezomib treatment. (Scale bar: 20 μm) **b**, Quantification of $CD138^+$ cell density corresponding to data in **a** ($n = 4$). "P" stands for PBS, "B" for bortezomib. Data are presented as mean ± s.d. *P* values were ~~analyzed~~analysed by an unpaired t-test.

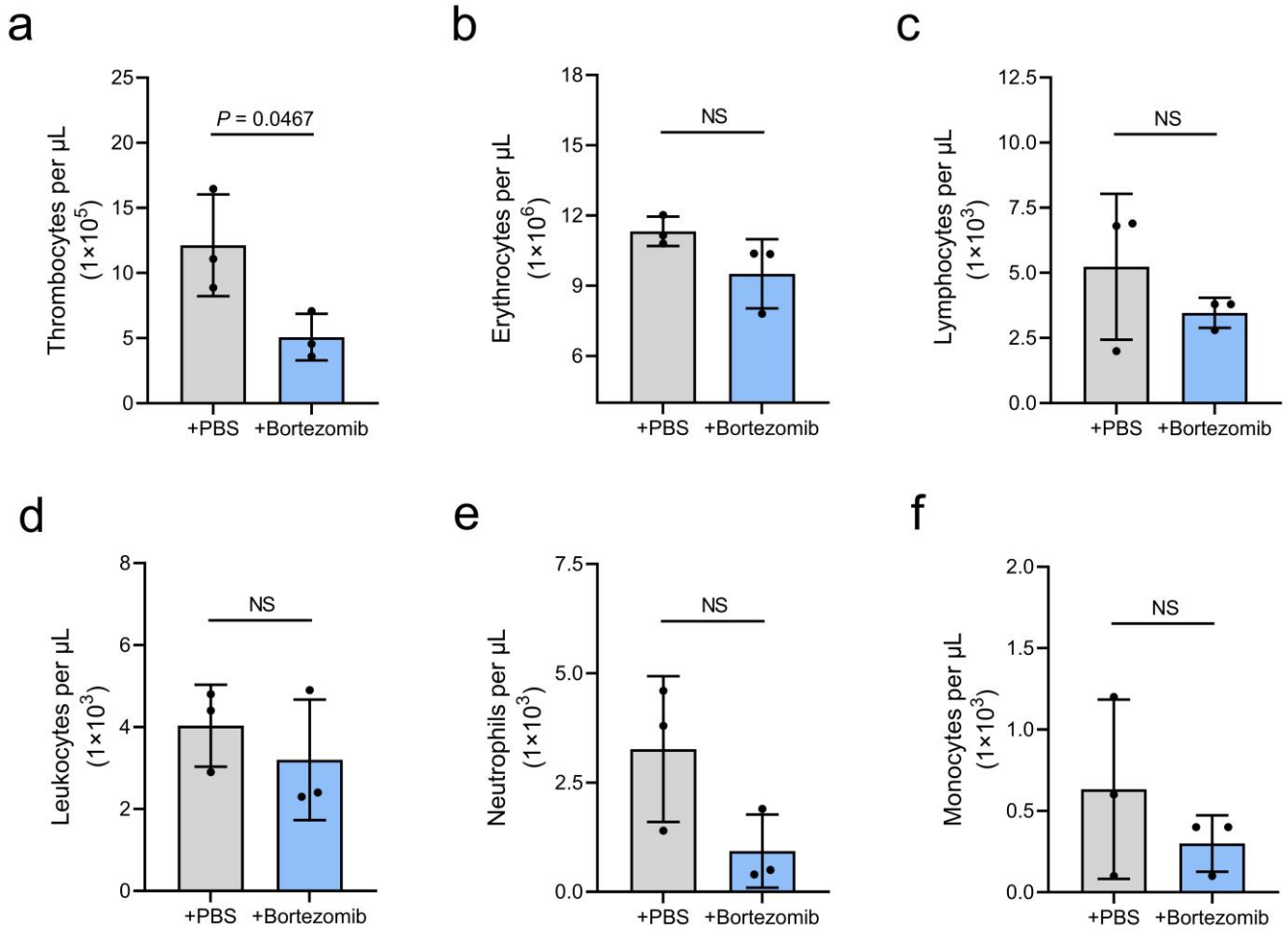

Supplementary Fig. ~~36~~37 | Effects of bortezomib treatment on peripheral blood cells. The count of **a**, thrombocytes, **b**, erythrocytes, **c**, lymphocytes, **d**, leukocytes, **e**, neutrophils, and **f**, monocytes in peripheral blood after treated with bortezomib~~.~~ (n = 3). Data are presented as mean ± s.d. P values were ~~analyzed~~analysed by an unpaired t-test. NS, not significant, P ~~>~~ ≥ 0.05.

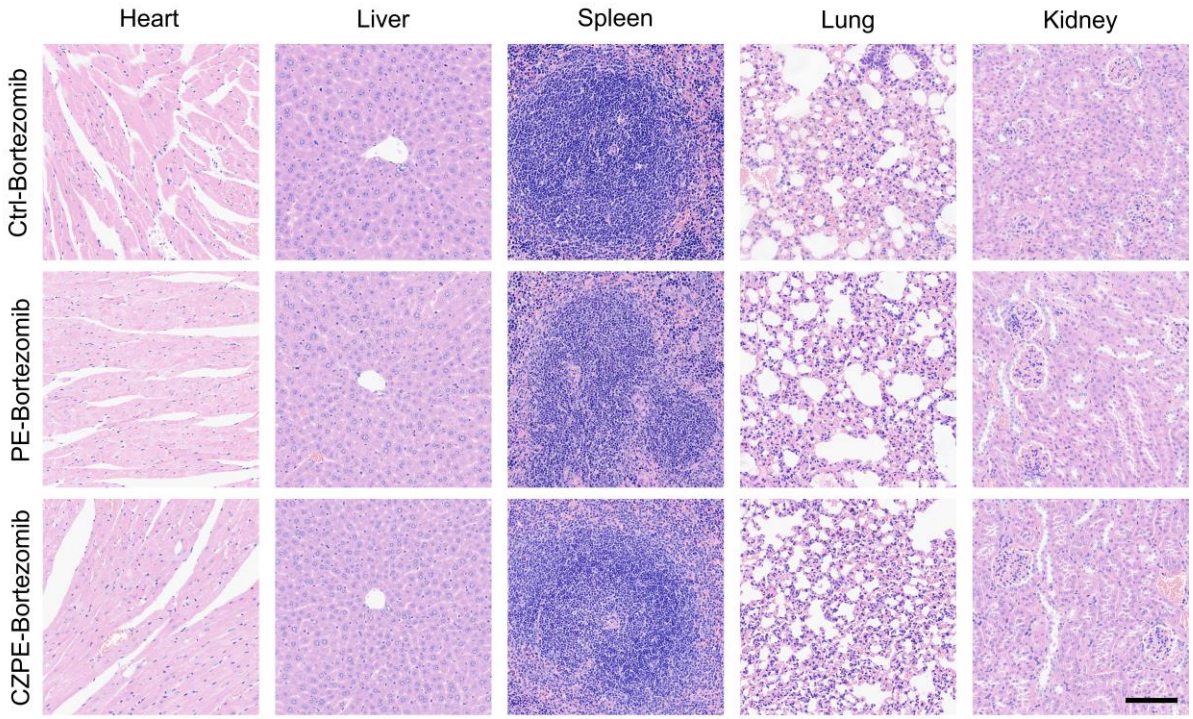

Supplementary Fig. ~~37~~38 | Histological analysis with H&E staining of major organ sections post bortezomib treatments. Sections include heart, liver, spleen, lung, and kidney. Scale bar, 100 μm.

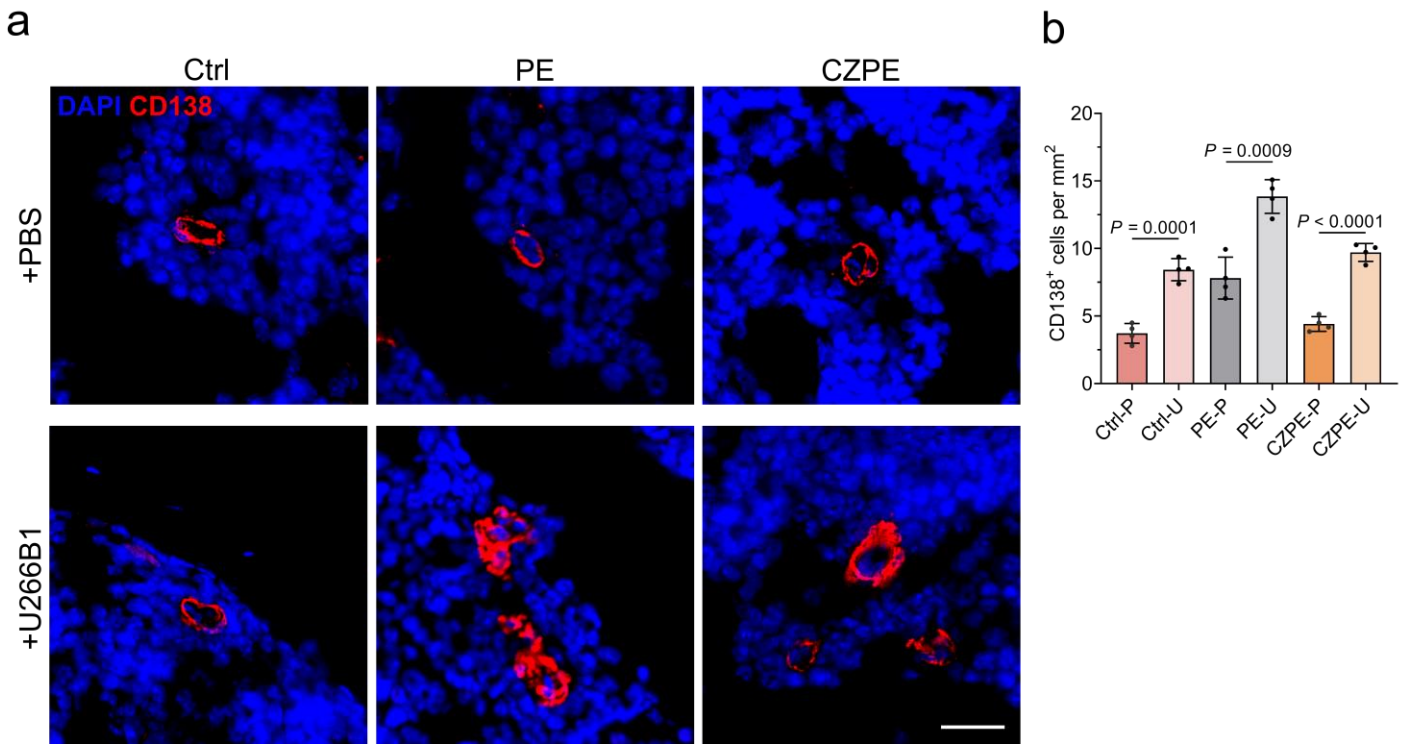

Supplementary Fig. ~~38~~39 | Infiltration of plasma cells in the peri-implant area after U266B1 cell injection. **a**, Representative immunofluorescence images staining of femoral sections after the injection of U266B1 cells. (Scale bar: 20 μm) **b**, Quantification of $CD138^+$ cell density corresponding to data in **a** ($n = 4$). "P" stands for PBS, "U" for U266B1 cells. Data are presented as mean ± s.d. *P* values were ~~analyzed~~analysed by an unpaired t-test.

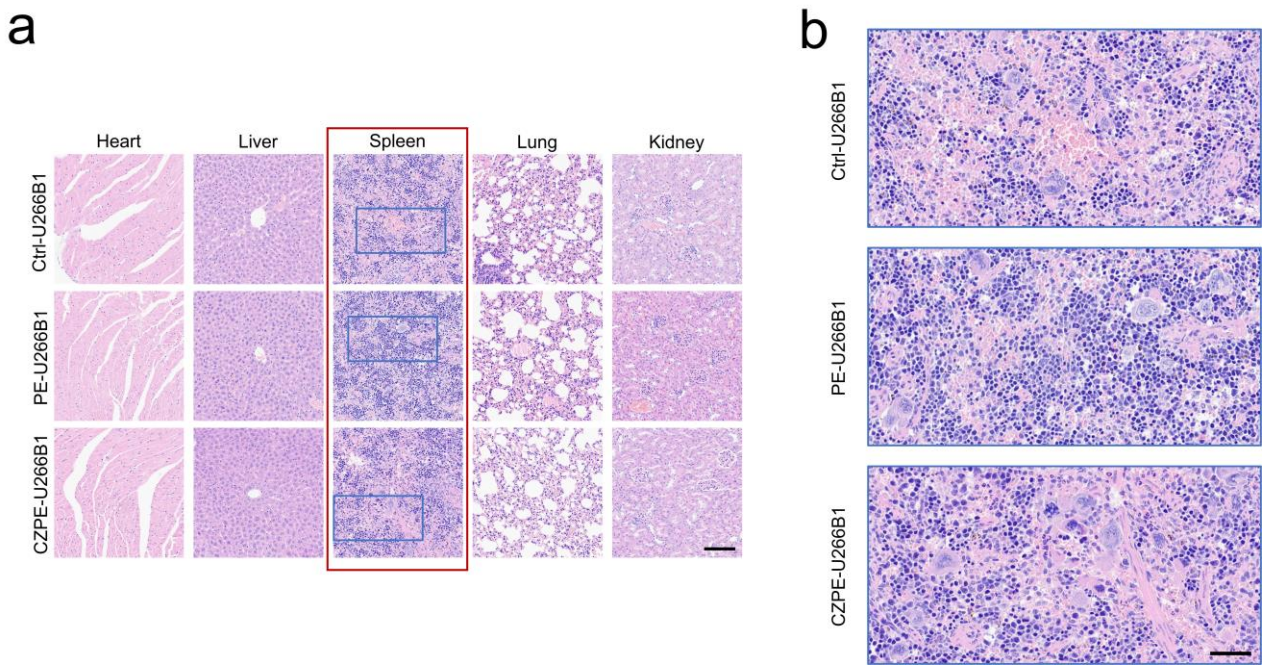

Supplementary Fig. ~~39~~40 | Histological analysis of major organ sections post U266B1 cells injections. a, H&E staining sections of heart, liver, spleen, lung, and kidney. Scale bar, 100 μm. **b**, Enlarged images of the blue boxed areas in **a**. Scale bar, 50 μm.

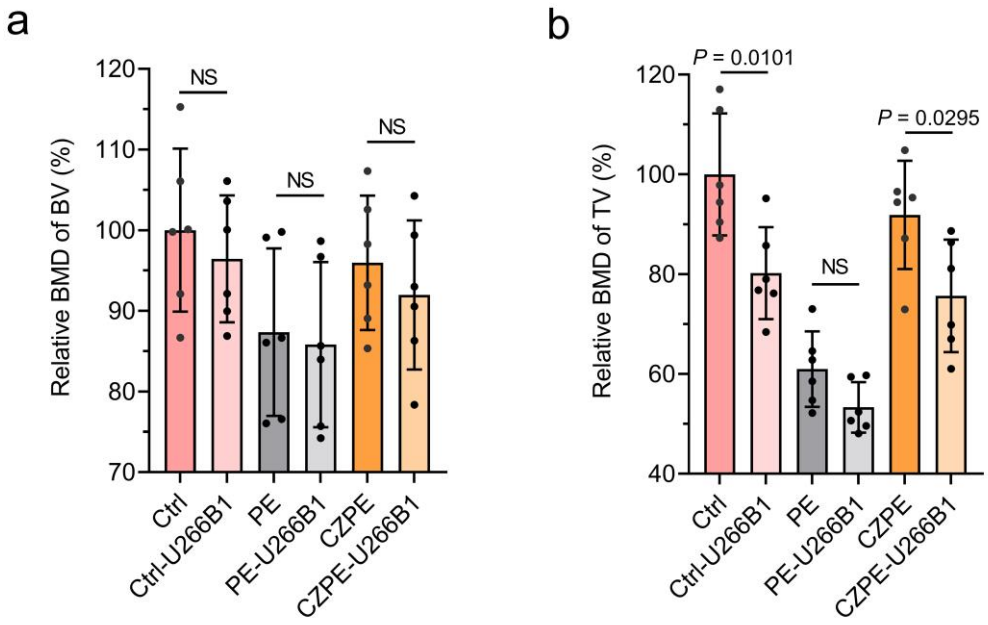

Supplementary Fig. ~~40~~41 | Femoral bone parameters of mice injected with U266B1 cells. a, Quantitative analysis of BMD of BV (n = 6). **b**, Quantitative analysis of BMD of TV (n = 6). Data are presented as mean ± s.d. P values were ~~analyzed~~analysed by an unpaired t-test. NS, not significant, $P \geq 0.05$.

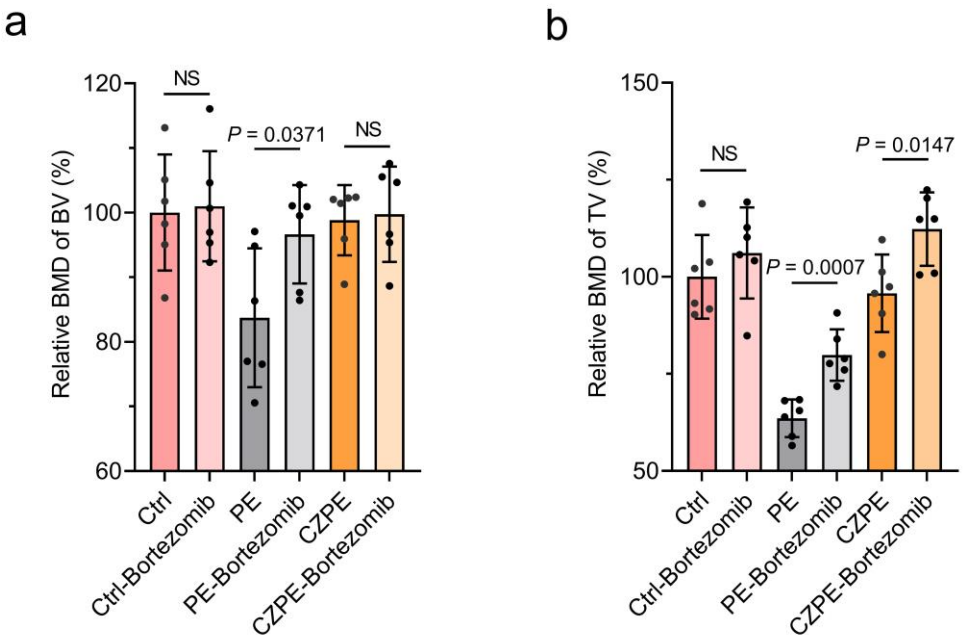

Supplementary Fig. ~~41~~42 | Femoral bone parameters of mice injected with bortezomib. a, Quantitative analysis of BMD of BV (n = 6). **b**, Quantitative analysis of BMD of TV (n = 6). Data are presented as mean ± s.d. P values were ~~analyzed~~analysed by an unpaired t-test. NS, not significant, $P \geq 0.05$.

Supplementary Table 1 Crystallinity for CZPE-1, CZPE-5, CZPE-10, and PE.

Samples	Enthalpy of crystallization (ΔHc) (10×J/g)	Degree of crystallinity (X_c) (%)
PE	17	58
CZPE-1	18	63
CZPE-5	19	69
CZPE-10	15	59

Supplementary Table 2 Summary of wear particle characteristics.

	Particles	ECD (μm)	AR	R
Smaller	PE	0.23 ± 0.09	1.83 ± 0.60	0.62 ± 0.19
	CZPE	0.22 ± 0.08	1.83 ± 0.53	0.65 ± 0.20
Larger	PE	2.92 ± 0.83	2.34 ± 0.55	0.39 ± 0.10
	CZPE	3.27 ± 1.05	2.25 ± 0.47	0.41 ± 0.10

Data are presented as mean ± s.d. (n = 5, 100 particles per sample)

Supplementary Table 3 Primers used ~~to~~for qRT-PCR.

Mouse	Forward primer	Reverse primer
~~*Gadph*~~*Gapdh*	TGGCCTTCCGTGTTCCTAC	GAGTTGCTGTTGAAGTCGCA
Il6	CCACTTCACAAGTCGGAGGCTTA	TGCAAGTGCATCATCGTTGTTC
Il1b	TCCAGGATGAGGACATGAGCAC	GAACGTCACACACCAGCAGGTTA
Tnf	ACTCCAGGCGGTGCCTATGT	GTGAGGGTCTGGGCCATAGAA
~~*Tnfsf11*~~	~~ATGGAAGGCTCATGGTTGGATGTG~~	~~GAGTGACTTTATGGGAACCCGATGG~~
~~*Ccl3*~~	~~CTCCCAGCCAGGTGTCATTTTCC~~	~~CAGGCATTCAGTTCCAGGTCAGTG~~
Sdc1	GGAAGTGCTGGGAGGTGTCATTG	CTGCCTTCGTCCTTCTTCTTCATCC
Nos2	CCAGCGGAGTGACGGCAAAC	GCAAGACCAGAGGCAGCACATC
Cd86	TCTGCCGTGCCCATTTACAAAGG	TGCCCAAATAGTGCTCGTACAGAAC
Mrc1	TGGCTTGGGCTACAGGAGAACC	TAGGCATGGCAGTGGCATTGATG
Human	Forward primer	Reverse primer
~~*GADPH*~~*GAPDH*	ACACCCACTCCTCCACCTTTG	TCCACCACCCTGTTGCTGTAG
IL6	GTGTTGCCTGCTGCCTTCC	TCTGAAGAGGTGAGTGGCTGTC
IL1B	ACGAATCTCCGACCACCACTAC	GCATCTTCCTCAGCTTGTCCATG
TNF	GTGGAGCTGGCCGAGGAG	AGGAGAAGAGGCTGAGGAACAAG
CD86	GTGGAACCAACACAATGGAGAGG	AAACACGCTGGGCTTCATCAG
NOS2	GGACCACATCTACCAGGAGGAG	CCAGGCAGGCGGGAATAGG
CD163	AAGAATCCCGCATTTGGCAGTG	AGAATAACTCCCGCATCCTCCTTG
SDC1	CTGCCGCAAATTGTGGCTAC	TGAGCCGGAGAAGTTGTCAGA
CCL3	CTGCCCTTGCTGTCCTCCT	GCAAGTGATGCAGAGAACTGGTT
TNFSF11	GGTGGATGGCTCATGGTTAG	GGTTGTACTGAAAATCGTTACC

Supplementary References

1 Nabiyev, A. A., Olejniczak, A., Pawlukojc, A., Balasoiu, M., Bunoiu, M., Maharramov, A. M., Nuriyev, M. A., Ismayilova, R. S., Azhibekov, A. K., Kabyshev, A. M., Ivankov, O. I., Vlase, T., Linnik, D. S., Shukurova, A. A., Ivanshina, O. Y., Turchenko, V. A. & Kuklin, A. I. Nano-ZrO_2 filled high-density polyethylene composites: Structure, thermal properties, and the influence γ-irradiation. *Polym. Degrad. Stabil.* **171**, 109042 (2020).

2 Chen, W., Bichara, D. A., Suhardi, J., Sheng, P. & Muratoglu, O. K. Effects of vitamin E-diffused highly cross-linked UHMWPE particles on inflammation, apoptosis and immune response against S. aureus. *Biomaterials* **143**, 46-56 (2017).

3 *Plastics - Determination of tensile properties*, ISO 527 (International Organization for Standardization, 2021).

4 *Standard Test Methods for Determining the Izod Pendulum Impact Resistance of Plastics*, ASTM D256-18 (American Society for Testing Materials, 2018).

5 Llorente, J., Román-Manso, B., Miranzo, P. & Belmonte, M. Tribological performance under dry sliding conditions of graphene/silicon carbide composites. *J. Eur. Ceram. Soc.* **36**, 429-435 (2016).

6 *Standard Test Method for Linearly Reciprocating Ball-on-Flat Sliding Wear*, ASTM G133-10 (American Society for Testing Materials, 2010).

7 *Standard Guide for Accelerated Aging of Sterile Barrier Systems for Medical Devices*, ASTM F1980-16 (American Society for Testing Materials, 2016).

8 *Standard Guide for Evaluating the Extent of Oxidation in Polyethylene Fabricated Forms Intended for Surgical Implants*, ASTM F2102-17 (American Society for Testing Materials, 2017).

9 Baxter, R. M., MacDonald, D. W., Kurtz, S. M. & Steinbeck, M. J. Characteristics of highly cross-linked polyethylene wear debris in vivo. *J. Biomed. Mater. Res. Part B* **101**, 467-475 (2013).

10 Liu, X., Wu, J., Liu, Q., Lin, A., Li, S., Zhang, Y., Wang, Q., Li, T., An, X., Zhou, Z., Yang, M. & Wei, H. Synthesis-temperature-regulated multi-enzyme-mimicking activities of ceria nanozymes. *J. Mat. Chem. B* **9**, 7238-7245 (2021).

11 Yang, Z., Luo, S., Zeng, Y., Shi, C. & Li, R. Albumin-mediated biomineralization of shape-controllable and biocompatible ceria nanomaterials. *ACS Appl. Mater. Interfaces* **9**, 6839-6848 (2017).

12 Dempster, D. W., Compston, J. E., Drezner, M. K., Glorieux, F. H., Kanis, J. A., Malluche, H., Meunier, P. J., Ott, S. M., Recker, R. R. & Parfitt, A. M. Standardized nomenclature, symbols, and units for bone histomorphometry: a 2012 update of the report of the ASBMR Histomorphometry Nomenclature Committee. *J. Bone Miner. Res.* **28**, 2-17 (2013).

13 Shea, K. G., Bloebaum, R. D., Avent, J. M., Birk, G. T. & Samuelson, K. M. Analysis of lymph nodes for polyethylene particles in patients who have had a primary joint replacement. *J. Bone Joint Surg. Am.* **78**, 497-504 (1996).

~~1~~14 Fang, H.-W., Ho, Y.-C., Yang, C.-B., Liu, H.-L., Ho, F.-Y., Lu, Y.-C., Ma, H.-M. & Huang, C.-H. Preparation of UHMWPE particles and establishment of inverted macrophage cell model to investigate wear particles induced bioactivites. *J. Biochem. Biophys. Methods* **68**, 175-187 (2006).

15 Liu, Y., Shi, F., Bo, L., Zhi, W., Weng, J. & Qu, S. A novel alginate-encapsulated system to study biological response to critical-sized wear particles of UHMWPE loaded with alendronate sodium. *Mater. Sci. Eng. C-Mater. Biol. Appl.* **79**, 679-686 (2017).

16 Lee, H.-p., Gu, L., Mooney, D. J., Levenston, M. E. & Chaudhuri, O. Mechanical confinement regulates cartilage matrix formation by chondrocytes. *Nat. Mater.* **16**, 1243-1251 (2017).

17 Gudipaty, S. A., Lindblom, J., Loftus, P. D., Redd, M. J., Edes, K., Davey, C. F., Krishnegowda, V. &

Rosenblatt, J. Mechanical stretch triggers rapid epithelial cell division through Piezo1. *Nature* **543**, 118-121 (2017).

18 Pavel, M., Renna, M., Park, S. J., Menzies, F. M., Ricketts, T., Füllgrabe, J., Ashkenazi, A., Frake, R. A., Lombarte, A. C., Bento, C. F., Franze, K. & Rubinsztein, D. C. Contact inhibition controls cell survival and proliferation via YAP/TAZ-autophagy axis. *Nat. Commun.* **9**, 2961 (2018).

19 Oral, E., Christensen, S. D., Malhi, A. S., Wannomae, K. K. & Muratoglu, O. K. Wear resistance and mechanical properties of highly cross-linked, ultrahigh-molecular weight polyethylene doped with vitamin E. *J. Arthroplasty* **21**, 580-591 (2006).

20 Jarrett, B. T., Cofske, J., Rosenberg, A. E., Oral, E., Muratoglu, O. & Malchau, H. In vivo biological response to vitamin E and vitamin-E-doped polyethylene. *J. Bone Joint Surg.* **92**, 2672-2681 (2010).

21 Bracco, P. & Oral, E. Vitamin E-stabilized UHMWPE for Total Joint Implants: A Review. *Clin. Orthop. Relat. Res.* **469**, 2286-2293 (2011).

22 Suhardi, V. J., Bichara, D. A., Kwok, S., Freiberg, A. A., Rubash, H., Malchau, H., Yun, S. H., Muratoglu, O. K. & Oral, E. A Fully Functional Drug-Eluting Joint Implant. *Nat. Biomed. Eng.* **1**, 0080 (2017).

23 Kapadia, B. H., Berg, R. A., Daley, J. A., Fritz, J., Bhave, A. & Mont, M. A. Periprosthetic joint infection. *Lancet* **387**, 386-394 (2016).

24 Cobelli, N., Scharf, B., Crisi, G. M., Hardin, J. & Santambrogio, L. Mediators of the inflammatory response to joint replacement devices. *Nat. Rev. Rheumatol.* **7**, 600-608 (2011).

25 Rodrigues, J. V. & Gomes, C. M. Enhanced superoxide and hydrogen peroxide detection in biological assays. *Free Radical Biol. Med.* **49**, 61-66 (2010).

26 Pajarinen, J., Kouri, V. P., Jämsen, E., Li, T. F., Mandelin, J. & Konttinen, Y. T. The response of macrophages to titanium particles is determined by macrophage polarization. *Acta Biomater.* **9**, 9229-9240 (2013).